JAAS

Sequential separation of cerium (Ce) and neodymium (Nd) in geological samples for high-precision analysis of stable Ce isotopes, stable and radiogenic Nd isotopes by MC-ICP-MS

Journal:	*Journal of Analytical Atomic Spectrometry*
Manuscript ID	JA-ART-12-2023-000451.R2
Article Type:	Paper
Date Submitted by the Author:	17-Apr-2024
Complete List of Authors:	Ding, Weiming; University of Minnesota Twin Cities, Earth and Environmental Sciences Zheng, Xin-Yuan; University of Minnesota Twin Cities, Earth and Environmental Sciences

Sequential separation of cerium (Ce) and neodymium (Nd) in geological samples for high-precision analysis of stable Ce isotopes, stable and radiogenic Nd isotopes by MC-ICP-MS

Weiming Ding, Xin-Yuan Zheng*

Department of Earth and Environmental Sciences, University of Minnesota-Twin Cities, Minneapolis, MN 55455, USA

*Corresponding author email: zhengxy@umn.edu

For submission to JAAS

Abstract

Stable isotopes of cerium (Ce) and neodymium (Nd), two rare earth elements (REEs), have emerged recently as useful tracers for a range of geological and environmental processes, such as redox changes in environments or continental weathering. However, the coupled use of stable isotopes of two (or more) rare earth elements is often hampered by difficulties in sequential separation of individual REEs and analysis of their stable isotope ratios at high precision. Here, we report a new three-stage chromatographic procedure that allows for simultaneous separation of Ce and Nd from geological samples for high-precision analysis of their stable isotope ratios on MC-ICP-MS. This approach also allows for analysis of radiogenic $^{143}Nd/^{144}Nd$ ratios at high precision. Sequential separation of Nd and Ce in our procedure was achieved and optimized using α-hydroxyisobutyric acid (α-HIBA) as an eluent. Possible Ce and Nd stable isotope fractionations induced by the α-HIBA column were quantified. Total procedural blanks of our three-stage separation are low for Ce (~46 pg) and Nd (~2 pg). Extensive tests were conducted on MC-ICP-MS under dry plasma conditions to evaluate matrix effects associated with common cationic impurities, acid concentration, analyte/dopant ratio, and concentration mismatch between the sample and the bracketing standards. The presence of α-HIBA, and, occasionally, aluminum (Al) can affect measurements of both stable Ce and Nd isotopes, and acid concentration mismatch may affect stable Nd isotope measurements. An iterative correction method was developed to considerably increase the tolerance of stable Ce isotope analysis to Nd isobaric interferences, thereby improving the robustness of our measurement. Based on analysis of various reference materials, we demonstrate that our new method is suitable for routine high-precision stable Ce and Nd isotope measurements on geological samples with a wide range of matrix compositions, yielding a long-term precision of ≤0.04‰ (2SD) for $^{142}Ce/^{140}Ce$ and ≤0.03‰ (2SD) for $^{146}Nd/^{144}Nd$. This method also permits accurate radiogenic $^{143}Nd/^{144}Nd$ measurement with an external precision of ≤15 ppm (2SD). Because the α-HIBA column is known for its capability of separating individual REEs, our approach can be adapted to separate other REEs for high-precision stable and radiogenic isotope analysis with minor modifications.

1 Introduction

Cerium (Ce) and neodymium (Nd) are lithophile and refractory rare earth elements (REEs). All REEs have a valence state of +3, whereas Ce has an additional +4 valence state and can transform between the two valence states in response to redox variations in environments. Because trivalent REEs have similar chemical properties that systematically vary from La to Lu, REE concentration patterns, often normalized to CI chondrites or Post Archean Australia Shales (PAAS)[1], can provide useful information on a variety of high- and low-temperature processes[2, 3]. In addition to typical adsorption/desorption processes affecting all trivalent REEs, redox transformations between soluble Ce^{3+} and less-soluble Ce^{4+} can also cause Ce concentration anomalies that can be discernible from REE patterns of natural samples[4-6]. This so-called "Ce anomaly" has been commonly used trace oxygen levels in ambient environments[7-10].

Isotope ratios of Ce and Nd can provide valuable information independent of REE concentration patterns on a wide range of geological and environmental processes. Cerium has four stable isotopes (^{136}Ce, ^{138}Ce, ^{140}Ce and ^{142}Ce), among which ^{138}Ce is radiogenic and a β^--decay product of ^{138}La ($t_{1/2}$ = 297 ± 28 Ga)[11]. Neodymium has seven stable isotopes (^{142}Nd, ^{143}Nd, ^{144}Nd, ^{145}Nd, ^{146}Nd, ^{148}Nd and ^{150}Nd), among which ^{142}Nd is a radiogenic daughter nuclide of the extinct ^{146}Sm via α-decay ($t_{1/2}$ = 103 Ma)[12, 13], and ^{143}Nd is a radiogenic product of α-decay of ^{147}Sm ($t_{1/2}$ = 106 Ga)[14]. There has been a long history of using radiogenic isotope ratios of Ce and Nd (i.e., $^{138}Ce/^{142}Ce$, $^{143}Nd/^{144}Nd$, $^{142}Nd/^{144}Nd$) to provide critical chronological constraints on geological events[15-18] and to investigate petrogenesis[19-28], oceanic circulation[29-31] and evolution of Earth and extraterrestrial bodies[13, 32-36].

Recently, there has been growing interest in potential applications of stable Ce and Nd isotopes (i.e., $^{142}Ce/^{140}Ce$ and $^{146}Nd/^{144}Nd$) to study geological, environmental, and cosmochemical processes. Measurements of glacial diamictites show that the upper continental crust has largely uniform stable Ce isotope ratios with little change through Earth history[37]. Resolvable variations of up to ~0.7‰ in $^{142}Ce/^{140}Ce$[38], however, have been observed in samples from low-temperature environments. Early measurements of natural ferromanganese deposits show that stable Ce isotopes are not a simple replica of

"Ce anomaly" but could provide unique geochemical information[38]. Pioneering experimental studies imply that stable Ce isotopes can be a promising tracer for redox transformations of manganese (Mn) in modern and ancient environments due to similar redox potential of Ce and Mn[39, 40], a claim supported by a recent study of stable Ce isotope variations in bauxite profiles[41]. This potential application is exciting because Mn oxidation in early oceans is notoriously challenging to pinpoint in geological records but has important implications for life evolution on Earth[42, 43]. Different from Ce, Nd does not have a redox chemistry. High-temperature magmatic processes, such as partial melting, typically do not produce resolvable stable Nd isotope fractionation[44, 45], but systematic variations of stable Nd isotopes have been observed in a weathering profile, possibly caused by isotopic fractionation during Nd adsorption/desorption on different mineral surfaces[46]. Stable Nd isotopes have also shown potential in elucidating sediment provenance[47] and petrogenesis[48, 49]. A combined use of stable Ce and Nd isotopes is anticipated to multiply the information that a single isotope system can offer, considering overall similar chemical behavior of the two elements but their distinct redox properties. This was demonstrated by a recent study that used multi-REE stable isotope ratios measured in meteoritic inclusions to infer heating events in the nascent solar system[50]. However, research that combines two or more stable REE isotopes to investigate low-temperature processes remains rare due to analytical challenges, although stable isotopic variations tend to be the largest in low-temperature surficial environments.

Several chromatographic methods have been established to separate Ce or Nd alone from geological samples for stable isotope analysis in the past few years (summarized in ESI Table S1), but only three of them have been demonstrated to be able to sequentially separate Ce and Nd from the same sample for stable Ce and Nd isotope analysis[50-53] (Table 1). One method is to first separate bulk REEs as a group using 2 mL Bio-Rad AG 50W-X8 resin, and then sequentially separates Ce and Nd using tandemly arranged columns, with the first column filled with 0.3 mL TRU Spec resin and the second one filled with ~1.25 mL LN Spec resin[51]. The total procedural Ce and Nd blanks reported for this method were relatively high (i.e., <1 ng) (Table 1), which may limit its use for low-REE samples. The second method capable of sequential Ce and

Nd separation for stable isotope analysis uses AG 50W-X12 resin to first separate bulk REEs from a sample, and then uses a single column filled with 2 mL DGA resin to separate Ce and Nd sequentially[52]. The third method for simultaneous separation of Ce and Nd relies on LN Spec resin, but it utilizes a fluoropolymer pneumatic liquid chromatography (FPLC) system comprising a long (i.e., 70 cm) chromatographic column filled with ~1.4 mL LN resin[50, 53]. Prepacked TODGA columns (2 mL resin) were used to separate REEs as a group before separation of individual REEs by the FPLC system. This FPLC system is advantageous in terms of its automation and demonstrated capability to sequentially separate 8 rare earth elements, including Ce and Nd, for stable isotope analysis. However, this system is not commercially available, and it uses a comparably large volume of eluent (e.g., ~80 mL HCl) that can potentially increase REE blanks. Also, the existing elution protocol on the FPLC system showed relatively low Nd yield (40%-70%) and, consequently, caused somewhat biased stable Nd isotope results for some geological reference materials via the simple sample-standard bracketing method[50, 53], possibly due to incomplete sample dissolution associated with the low-molarity acid used for FPLC separation. As a result, the more complicated double spike technique is preferred for Nd separation[53]. Although all three methods have proven effective in sequential Ce and Nd separation from geological samples in support of high-precision stable isotope measurements of the two elements, they all use relatively large amount (~1.4–2 mL) of expensive specific resins (i.e., LN or DGA).

It is known that ammonium-form (NH_4^+) cation exchange resin and α-hydroxyisobutyric acid (α-HIBA) can provide excellent separation for individual REEs in a reversed order[54, 55], and different elution protocols based on α-HIBA solution have been developed and widely utilized for purifying Ce or Nd from geological samples for high-precision radiogenic isotope measurements[15, 28, 32, 35, 36, 56-63]. This method uses the conventional cation exchange resin to separate Ce and Nd, so it can lower the cost of Ce-Nd separation. However, no attempt has been made so far to explore the potential of the α-HIBA method in preparing geological samples for stable Ce and Nd isotope analyses. Because stable isotope analysis requires a quantitative recovery of the target element from the separation and sufficient removal of matrix elements,

both of which are not necessarily required by analysis of radiogenic isotope ratios, it remains unknown if an α-HIBA-based chromatographic separation protocol can be developed to simultaneous prepare Ce and Nd for stable isotope analyses.

In this study, we developed a new three-stage chromatographic procedure for simultaneous Ce and Nd separation for high-precision stable isotope measurements on MC-ICP-MS. For the first time, we demonstrate that the α-HIBA method, the key stage of our procedure responsible for Ce-Nd separation, is capable of supporting routine high-precision measurements of stable Nd and Ce isotopes in geological samples of diverse matrix compositions with consistently high yields after chromatography. We also conducted extensive tests to evaluate several important factors that may affect stable Nd and Ce isotope analysis on MC-ICP-MS and optimized the analytical protocol on the mass spectrometer based on our test results. Importantly, our approach for chromatographic separation and stable isotope analysis on MC-ICP-MS does not compromise high-precision radiogenic Nd isotope measurements. Our results also indicate that the α-HIBA method can be extended with minor modifications to simultaneously separate other REEs beyond Ce and Nd for both stable and radiogenic isotope analyses in future.

2 Experimental section

2.1 Nomenclature, reagents, and materials

Stable Ce and Nd isotope compositions are expressed by the conventional δ-notation relative to NIST 3110 Ce solution and JNdi-1 Nd solution, respectively (Eq. 1 and 2).

$$\delta^{142}Ce = \left(\frac{^{142}Ce/^{140}Ce_{sample}}{^{142}Ce/^{140}Ce_{NIST\ 3110}} - 1\right) \times 1000 \quad (1)$$

$$\delta^{X}Nd = \left(\frac{^{X}Nd/^{144}Nd_{sample}}{^{X}Nd/^{144}Nd_{JNdi-1}} - 1\right) \times 1000 \quad (2)$$

where ***X*** represents a specific stable Nd isotope mass, including 145, 146, 148, or 150. For simplicity, we used $^{146}Nd/^{144}Nd$ as an example of stable Nd isotopes here, but other stable Nd isotope ratios were also analyzed.

Sample dissolution and preparation were conducted in a class-100 (ISO Class 5 equivalent) clean lab in the Department of Earth and Environmental Sciences, University of Minnesota. Milli-Q water (18.2 MΩ-cm) and Optima™ grade (Fisher Scientific) acids or house-distilled acids of comparable purity were used for sample digestion and chromatographic separation in this study. α-Hydroxyisobutyric acid (99%, solid) was purchased from MilliporeSigma and then purified prior to use. Optima™ grade ammonia solution was used to adjust pH of α-HIBA solution and to convert H^+-form cation exchange resin (Bio-Rad AG50W-X4) to NH_4^+ form. Details of α-HIBA solution preparation, including purification and pH adjustment, and conversion of cation exchange resin to its NH_4^+ form can be found in the ESI. An in-house multi-REE solution and several dissolved rock standards (BCR-2, AGV-2a, and BHVO-2) were used for column calibration. The multi-REE solution was prepared to have a seawater-like REE pattern by gravimetrically mixing 14 single rare earth element solutions from High-Purity Standards (South Carolina, USA).

Four pure Ce solutions were used in this study. NIST SRM 3110 solution was used as the bracketing standard during our stable Ce isotope analysis. Three other in-house Ce solutions (UMN Ce-I, II, and III) were routinely analyzed in our laboratory to assess the long-term reproducibility of our $^{142}Ce/^{140}Ce$ measurement. UMN Ce-I is a pure Ce solution (10,000 μg/mL in 4% HNO_3, source: $Ce_2(CO_3)_3 \cdot XH_2O$) purchased from High-Purity Standards. UMN Ce-II was made by dissolving cerium nitrate hexahydrate salt ($(Ce(NO_3)_3 \cdot 6H_2O$, 99.999% purity) in 2% HNO_3, and UMN Ce-III was made by dissolving cerium chloride heptahydrate salt ($CeCl_3 \cdot 7H_2O$, 99.999% purity) in 2% HNO_3. Both high-purity salts were purchased from

MilliporeSigma. Three pure Nd solutions were used for stable and radiogenic Nd isotope analysis, including JNdi-1, and two in-house Ames-I and Ames-II Nd solutions. JNdi-1 is an international standard for radiogenic $^{143}Nd/^{144}Nd$ ratios[64], and it is also used as the bracketing standard for stable Nd isotope analysis. Our Ames-I and Ames-II Nd solutions were obtained from University of Wisconsin–Madison, and their radiogenic $^{143}Nd/^{144}Nd$ ratios have been routinely analyzed at UW–Madison for more than a decade [63, 65].

Nine geological reference materials from US Geological Survey (USGS) and Geological Survey of Japan (GSJ) were used to validate accuracy of our Ce and Nd isotope measurements. These materials include 2 basalts (BCR-2, BHVO-2), 1 andesite (AGV-2a), 1 carbonatite (COQ-1), 1 granodiorite (GSP-2), 1 mica schist (SDC-1), and 3 manganese nodules (NOD-A-1, NOD-P-1, JMn-1). Powders of geological reference materials (~50-100 mg) were weighted into pre-cleaned Savillex Teflon vials, and then dissolved with a mixture of concentrated HNO_3 and HF (1:3, v/v) on a Teflon-coated graphite hotplate at ~150℃ for at least 48 hours. Samples were then evaporated to dryness, followed by repeated boiling in concentrated HCl until all solid residues were fully dissolved. The digestion step by the concentrated HNO_3 and HF mixture were repeated if any residues were found visible in concentrated HCl.

2.2 Chromatographic separation

We developed a new 3-stage chromatographic separation procedure that could purify Ce and Nd from the same sample for stable isotope analysis. The details of the procedure are summarized in Table 2.

The first column separates all REEs as a group from sample matrices, using Bio-Rad AG50W-X8 resin (H^+ form, 200-400 mesh) and Bio-Rad Poly-Prep columns with 2 mL resin bed (Fig. 1A). Samples are loaded onto the resin in 1 mL of 2 M HCl and then eluted with 30 mL of 2 M HCl to remove major and trace matrix elements (e.g., Na, Mg, Al, Ca, Fe, Rb, Sr). Subsequently, the REEs fraction is collected in 28 mL of 6 M HCl. A wider window of 6 M HCl than the Ce and Nd peaks shown in Fig. 1A was intentionally collected to ensure complete recovery of Ce and Nd against any possible matrix-dependent tailing of Ce and Nd elution peaks during preparation of different geological samples, and it also allows for a full recovery of La

that can facilitate future applications of the La-Ce geochronology if needed. The bulk REE fraction was dried down at 140℃ and then re-dissolved in 0.4 mL of 0.1 M HCl for the second stage separation.

The second column separates Ce and Nd sequentially from other REEs and Ba, using AG50W-X4 resin (NH_4^+ form, 200-400 mesh) pre-equilibrated with 0.150 M α-HIBA solution and custom-built borosilicate glass columns (resin bed length = 29.3 cm, inner diameter = 0.3 cm) (Fig. 1B), following the elution protocol detailed in Table 2. The separation was conducted under atmospheric pressure without use of any pressurized device. Purified Nd and Ce cuts were dried down at 130℃ and then re-dissolved in 1 mL of 4 M HNO_3 for a final clean-up step using small columns.

The third column is designed to remove residual α-HIBA in the Ce or Nd fraction from the second column, using house-made small Teflon columns (length = 2.1 cm, inner diameter = 0.4 cm) and Eichrom DGA resin (50-100 μm) (Fig. 1C). To effectively remove α-HIBA compounds from Ce or Nd, it is desirable to conduct the separation at a relatively high acid molarity that should better promote dissociation of REE–α-HIBA complexes. Given this consideration, DGA resin was chosen to take advantage of the fact that REEs are more strongly adsorbed on this resin in acids of higher molarities[66]. This unique REEs partitioning behavior on the DGA resin should facilitate more effective removal of α-HIBA anions/molecules from Ce or Nd cations on the column. Only ~0.26 mL DGA resin is used for each sample, considerably less than the amount (i.e., ~1.4 to 2 mL) required for previous separation methods based on DGA or LN resins[50-53]. Residual α-HIBA is effectively removed by eluting the column with 4 M HNO_3, and Ce or Nd is quantitatively recovered in 6 mL of 0.1 M HCl (details in Section 3.3.4). After purification, the Ce or Nd cut is dried and re-dissolved in 2% (v/v) HNO_3 for isotopic analysis.

Tests were conducted to examine column yields and blank levels for Ce and Nd, and the test samples were analyzed by a Thermo iCAP™ Triple Quadrupole (TQ-) ICP-MS in the Department of Earth and Environmental Sciences, University of Minnesota. The yield of Ce or Nd was quantified by passing a known amount of a multi-REE solution with known REE concentrations through the entire 3-stage separation. The total procedural yields were determined to be >99% for both Ce and Nd. The Ce and Nd

yields measured in these tests are consistent with the yields measured during our experiments designed to quantify column-induced stable Ce and Nd isotope fractionation (see Section 3.1.2). Quantitative Ce and Nd yields of our new procedure are further supported by accurate stable Ce and Nd isotope compositions measured for a wide range of reference materials that were processed by this new method (see Section 3.4). The total procedural blank of our chromatographic separation is 46 pg (n = 3) for Ce and 2 pg (n = 3) for Nd, among the lowest blank levels compared to other published methods (Table 1), if not the lowest.

2.3 Instrument configurations

Isotope ratios of Ce and Nd were measured on a collision-cell MC-ICP-MS "Sapphire" (Nu Instruments, Serial No. SP006) coupled with an Apex Omega HF desolvator and a Teflon nebulizer (~100 μL/min, Elemental Scientific) in the Department of Earth and Environmental Sciences, University of Minnesota. In this study, all isotope analyses were conducted using the conventional high-energy ion path with an acceleration voltage of 6 kV and RF power of 1300 W at low mass resolution. Isotope ratios were collected in static mode, and relevant faraday cup configurations are listed in Table 3. Typical instrument operating settings are compiled in Table 4.

High-purity N_2 gas was added via Apex desolvator to keep $^{140}Ce^{16}O^+/^{140}Ce^+$ ratios below 0.05%. Although a higher Ce sensitivity could be obtained on our MC-ICP-MS without use of N_2, lower oxide formation was preferred in our study, because oxide formation may degrade the precision of Ce isotope analysis[67]. Typically, 100 ng/mL Ce doped with 200 ng/mL Sm were used during the stable Ce isotope measurement, yielding ion intensity of >15 V on ^{140}Ce and >1.4 V on ^{144}Sm. Similarly, N_2 gas was used to keep $^{142}Nd^{16}O^+/^{142}Nd^+$ ratios below 0.1% during stable and radiogenic Nd isotope measurements. Typically, 50 ng/mL Nd doped with 25 ng/mL Eu was used during Nd isotope measurement, yielding ion intensity of > 4 V on ^{142}Nd, > 4 V on ^{153}Eu. Concentrations between the sample and the bracketing standard are typically matched within 5% as a precaution, even though our tests demonstrated that concentration mismatch had negligible effect on stable Ce and Nd isotope measurements (details in Section 3.3.1). Four NIST 3110 Ce

solutions with varying concentrations (-50%, -25%, +25%, +50% relative to the bracketing standard) were measured routinely at the beginning of each analytical sequence to evaluate the effect of concentration mismatch. Each analysis was preceded by an on-peak-zero (OPZ) measurement of blank 2% HNO_3, and the measured OPZ intensities were subtracted from the intensities obtained in the subsequent analyte measurement.

The combined standard-sample bracketing and internal normalization (C-SSBIN) method was used in our stable Ce and Nd isotope measurements to correct for instrumental mass bias. Data were also processed using the simple standard-sample bracketing (SSB) method for a direct comparison to the C-SSBIN approach (details in Section 3.2.1). Samarium was selected as the internal standard during stable Ce isotope analysis, and a $^{148}Sm/^{144}Sm$ ratio of 3.6612[68] was used for mass bias correction. ^{145}Nd was monitored simultaneously during the measurement to correct for possible isobaric interferences on ^{142}Ce from ^{142}Nd. For stable Nd isotope, Eu was used to correct for mass bias, using $^{153}Eu/^{151}Eu = 1.0916$[68]. ^{147}Sm was measured to correct for possible isobaric interferences of Sm isotopes on Nd isotopes, although the correction for geological samples was typically negligible due to effective separation of Sm and Nd by our chromatographic procedure (Sm/Nd ratios < 0.02%) (Fig. S10). Limited by mass dispersion of the instrument, ^{140}Ce cannot be simultaneously measured with Nd isotopes in our current cup configuration. This prevents monitoring of potential ^{142}Ce interference on ^{142}Nd during our analysis. We observed that residual Ce absorbed on the permeable expanded polytetrafluoroethylene (EPTFE) membrane inside the Apex desolvator could sporadically produce erroneous $^{142}Nd/^{144}Nd$ measurements when Nd isotope analysis was performed immediately after an analytical session of Ce isotopes without thorough cleaning of the Apex membrane. As a result, we do not report stable $^{142}Nd/^{144}Nd$ ratios here. Radiogenic $^{143}Nd/^{144}Nd$ ratios can be obtained simultaneously with stable Nd isotope analyses, and raw $^{143}Nd/^{144}Nd$ ratios were corrected for mass bias using the exponential law and $^{146}Nd/^{144}Nd$ of 0.7219. Internally corrected $^{143}Nd/^{144}Nd$ ratios of samples were further corrected externally by normalizing $^{143}Nd/^{144}Nd$ of the JNdi-1 bracketing standard to a recommended value of 0.512115[64]. This value was preferred because it was anchored by the

recommended $^{143}Nd/^{144}Nd$ ratio of 0.511858 for the earlier international standard for radiogenic Nd isotope isotopes – La Jolla[64].

3 Results and discussion

3.1 Assessment and optimization of the α-HIBA chemistry

3.1.1 Elution optimization for the α-HIBA column

Although it is known that the α-HIBA method can separate REEs, previous studies that used this approach mostly focused on purifying rare earth elements, primarily Nd, for radiogenic isotope analysis[15, 28, 32, 35, 36, 56-63, 69, 70]. It is unknown if any of the published elution protocols could work for stable Ce and Nd isotope analysis, because quantitative column yields and sufficient removal of matrix elements are essential for stable isotope analysis but less critical for radiogenic isotope analysis.

Multiple tests were conducted to establish the elution protocol of our α-HIBA column – the key stage responsible for sequential separation of Nd and Ce in our procedure. Using in-house high-purity multi-REE solution as a test sample, we first established elution curves using α-HIBA solutions (pH = 4.68 ± 0.02) of 6 different concentrations that ranged from 0.100 M to 0.225 M (ESI Fig. S1–S6), as well as using combinations of 0.150 M and 0.225 M α-HIBA solutions (ESI Fig. S7–S8). Elution results show that either 0.225 M or a combination of 0.150 M and 0.225 M α-HIBA solutions can be effective for the Nd and Ce separation. To further compare these two elution protocols derived from the high-purity multi-REE solution and test if elution curves can be altered by different sample matrices, three USGS rock standards (BCR-2, BHVO-2, AGV-2a) were first passed through the first-stage column to separate bulk REEs, and then through the second-stage α-HIBA column using the two different elution protocols. Both Nd and Ce were collected, along with 3 pre-cuts (0.4 mL each) and 3 post-cuts (0.4 mL each) relative to Nd and Ce cuts. All solutions were measured for Sm, Nd, and Ce concentrations on TQ-ICP-MS to evaluate the degree of separation among neighboring REEs. The Nd cuts were also analyzed on MC-ICP-MS to evaluate whether or not they were pure enough for accurate radiogenic $^{143}Nd/^{144}Nd$ measurements.

Although results based on the high-purity multi-REE solution showed that either of the two tested elution protocols should be effective, results from rock standards revealed significantly high Sm/Nd mass ratios in the Nd cut with a low Nd yield (<60%) and significantly high Nd/Ce mass ratios in the Ce cut, when only 0.225 M α-HIBA solution was used as the eluent (Fig. 2A and 2C). This suggests changes in the elution curve that caused significant tailing of Sm into the Nd cut and of Nd into the Ce cut. Unsurprisingly, the measured $^{143}Nd/^{144}Nd$ ratios of the three standards also deviated significantly from recommended values due to intense isobaric interferences of ^{144}Sm on ^{144}Nd (ESI Fig. S9). Although stable Nd and Ce isotopes were not analyzed in this test, Nd/Ce levels found in the Ce cut were much higher than the threshold that can be tolerated during our Ce isotope measurements (Details in Section 3.2.2) (Fig. 2C and 5). In contrast, the elution by 0.150 M α-HIBA followed by 0.225 M α-HIBA yielded consistently low Sm/Nd and Nd/Ce mass ratios in the Nd cut and Ce cut, respectively, regardless sample types (i.e., basalt *vs.* andesite) (Fig. 2B and 2C). Also, the measured radiogenic $^{143}Nd/^{144}Nd$ ratios of the three rock standards were accurate (ESI Fig. S9). Our results demonstrate that elution by α-HIBA solution with a single molarity of 0.225 M can cause significant tailing of REE elution peaks during preparation of geological samples, and, hence, it is not suitable for preparing geological samples for stable Ce and Nd isotope analysis. As a result, we adopted an elution protocol using a combination of 0.150 M and 0.225 M α-HIBA. The robustness of our separation procedure is shown by the excellent long-term reproducibility of stable Ce and Nd isotopes, and radiogenic $^{143}Nd/^{144}Nd$ ratios measured for geological reference materials of a wide range chemical compositions (Fig. 11 and 12). In addition to Nd and Ce, our elution experiments using various concentrations of α-HIBA solutions also show the promise of the α-HIBA chemistry in separating other rare earth elements, such as Sm (ESI Fig. S3 and S4), Eu and Gd (ESI Fig. S2), in support of stable isotope analysis, although further validation is needed in future.

3.1.2 Stable Ce and Nd isotope fractionation on the α-HIBA column

Stable Ce and Nd isotope fractionation factors on the α-HIBA column were quantified in this study, providing a necessary framework that allows for assessment of possible influence of incomplete yield from our column on stable Ce and Nd isotope analysis. Column-induced stable Ce isotope fractionation has been quantified for chromatographic methods using LN and DGA resin[51, 71, 72], but it has never been quantified for the α-HIBA column. Stable Nd isotope fractionation during the α-HIBA chemistry has been studied[69]; a ~1.40‰ difference in δ^{146}Nd was observed between the head and tail of the Nd elution peak, with heavier Nd isotopes being eluted first relative to lighter isotopes. However, this previous study used columns of different physical sizes compared to ours, so it is unclear if the observed stable Nd isotope fractionation applies to our column.

In our experiments, NIST 3110 Ce (a total of 495.3 ng Ce) and JNdi-1 (501.9 ng Nd) were individually processed through the α-HIBA column using our established elution protocol. Instead of collecting Ce or Nd as a single cut, Ce and Nd were sequentially collected into 8 separate fractions and 6 fractions, respectively. All fractions were then purified by the third-stage column to remove residual α-HIBA, followed by stable Ce or Nd isotope analysis on MC-ICP-MS.

Based on the measured Ce and Nd concentrations in individual fractions, it was calculated that a total of 497.93 ng Ce and 495.76 ng Nd was recovered (ESI Table S2 and S3), representing a yield of 100% for Ce and 99% for Nd through our combined second-stage α-HIBA column and the third-stage small DGA column. Cumulative δ^{142}Ce and δ^{146}Nd values based on isotope mass balance calculations and the measured concentration and isotopic data from individual samples were -0.029‰ and 0.023‰, respectively (ESI Table S2 and S3), demonstrating quantitative recoveries of Ce and Nd during our experiments. Isotopic differences observed in individual fractions collected from our experiments, therefore, truly reflect stable isotope fractionation induced on our α-HIBA column. The isotopic results show that heavier isotopes are preferentially eluted from our α-HIBA column for both Ce and Nd (Fig. 3). The isotopic difference between the first and last fractions collected from the column is 1.00‰ for δ^{142}Ce and 1.09‰ for δ^{146}Nd.

Stable Ce isotope fractionation factor on our α-HIBA column can be estimated using the theory of chromatography[73, 74]. The theory predicts that the slope of the linear regression line derived from $\ln((^{142}Ce/^{140}Ce)_{fraction}/(^{142}Ce/^{140}Ce)_{NIST\ 3110})$ and accumulative eluted percent of Ce is equivalent to $\varepsilon\sqrt{N}$, where ε is the single-step ("batch") enrichment factor, and N is the number of theoretical plates in the column. N can be estimated from the experimental data through the following equation:

$$N = 2\pi\left(\frac{c_{max}\bar{v}}{100\%}\right)^2 \quad (3)$$

where c_{max} is the maximum peak height, defined by the percentage of Ce collected at the elution peak normalized to a unit volume (i.e., % Ce/mL), and $\bar{v}$ is the peak elution volume. Although Ce was eluted in 0.225 M α-HIBA, the volume of 0.150 M α-HIBA solution prior to Ce elution (i.e., 2.8 mL) should be also included in the $\bar{v}$ calculation, because Ce distribution coefficients on the resin under these two molarities are similar (<10 times)[75]. Based on our results, the peak elution volume ($\bar{v}$) of Ce is located in the 13.6-14 mL fraction. An average volume value of 13.8 mL was accordingly selected as the estimate of $\bar{v}$. 26.29% of total Ce mass relative to total Ce mass loaded to the column was collected in this 0.4 mL cut (Fig. 1B). Based on the theory by Glueckauf (1955, 1958)[73, 74], c_{max} value can be calculated as 65.7 %/mL. The number of theoretical plates N then can be calculated to be ~516 for Ce based on Eq. 3. As a result, the enrichment factor ε for $^{142}Ce/^{140}Ce$ on our α-HIBA column is estimated to be 1.5×10^{-5} at room temperature of 19.4 ± 0.3℃ (Fig. 3A). Similar calculations were also performed for Nd, yielding the peak elution volume ($\bar{v}$) of 7.8 mL for Nd within 7.6-8 mL, a c_{max} value of 122.8 %/mL, and N of ~576. Hence, the enrichment factor in $^{146}Nd/^{144}Nd$ on our α-HIBA column was estimated to be 1.5×10^{-5} at room temperature of 19.4 ± 0.3℃ (Fig. 3B).

More gentle slope of a regression line in Fig. 3 indicates smaller column-induced isotopic fractionation. Although different columns and elution protocols were developed in this and previous studies, column-induced Ce and Nd isotope enrichment factors are broadly comparable among different separation methods using LN resin and the α-HIBA chemistry[51, 69]. Despite the high cost, the method based on DGA resin[71, 76,

^{77} produces the smallest Ce and Nd isotope fractionations (Fig. 3), thereby is more resistant to potential Ce and Nd loss from the column. Given our results that demonstrated measurable column-induced stable isotope fractionation (Fig. X), quantitative yields of Ce and Nd from our α-HIBA column are, therefore, essential for accurate measurements of stable Ce and Nd isotopes.

3.2 Correction for instrumental mass bias and isobaric interferences

3.2.1 Instrumental mass bias correction

The simple sample-standard bracketing (SSB) method[78, 79] and the combined sample-standard bracketing and internal normalization (C-SSBIN) method[80, 81] are two methods commonly used to correct for instrumental mass bias during stable isotope analysis on MC-ICP-MS. The C-SSBIN method has been applied to analysis of stable Ce isotopes (with Sm-doping)[37-41, 51, 52, 67, 71, 76, 82] and stable Nd isotopes (with Eu-doping)[46, 51, 52, 83, 84], whereas the simple SSB method has also been adopted by some studies for stable Nd isotope analysis[47, 72, 85, 86]. Compared to the simple SSB method, the C-SSBIN method requires addition of a dopant element in each sample and the bracketing standard for the measurement, so it is more labor-intensive and accompanied with a higher risk of sample contamination. Yet, a direct comparison of C-SSBIN and simple SSB methods for stable Ce and Nd isotope measurements is absent in literature, making it difficult to determine if the additional internal normalization associated with the C-SSBIN method indeed offers any analytical benefit.

In this study, we provided the first direct comparison of the two correction methods for stable Ce and Nd isotope analyses, based on data collected over a >1-year period. During our tests, samples were doped with high-purity Sm during stable Ce isotope analysis, or with high-purity Eu during stable Nd isotope analysis. Data were processed using (1) a simple SSB method where the measured Ce (or Nd) stable isotope ratio of a sample was normalized to the average of the two adjacent bracketing standard measurements, and (2) a C-SSBIN method where the measured Ce (or Nd) stable isotope ratios were first internally corrected using

$^{148}Sm/^{144}Sm$ = 3.6612 (Eu/Eu = 1.0916) and an exponential law, and then externally corrected following the same way as the simple SSB method.

As shown in Fig. 4, our comparison clearly demonstrates that use of a C-SSBIN method can significantly improve precision of stable Ce and Nd isotope analysis compared to use of a simple SSB method. Regardless pure solutions or geological materials, the C-SSBIN method yielded precision consistently better than 0.04‰ (2SD) for $^{142}Ce/^{140}Ce$, whereas a simple SSB method gave variable and frequently worsened precisions ranging from 0.01‰ to 0.32‰ (Fig. 4A). Through the C-SSBIN method, the best achieved long-term precision (> 7 months) is 0.02‰ (2SD, N=19) in $^{142}Ce/^{140}Ce$ for pure UMN Ce-I solution. Similar findings were also observed for stable Nd isotopes (Fig. 4B). The improved long-term precision associated with the C-SSBIN method implies that isotopic mass bias of the dopant element closely followed the mass bias of Ce or Nd isotopes during our MC-ICP-MS measurements. Normalizing the measured isotope ratios of the dopant element to a fixed value prior to the simple SSB mass bias correction, therefore, helped to effectively smooth out possible subtle differences in instrumental mass bias between sample measurements and adjacent measurements of the bracketing standard. Our results support that the C-SSBIN method is superior to the simple SSB method in terms of mass bias correction during stable Ce and Nd isotope measurements on MC-ICP-MS.

3.2.2 Correction for isobaric interferences during Ce and Nd isotope analysis

Isobaric interferences should be closely monitored and, if necessary, corrected during the measurement of stable Ce and Nd isotope compositions. Stable Ce isotope measurements can be affected by (1) interferences of ^{142}Nd on ^{142}Ce, and (2) interferences of ^{144}Nd and ^{148}Nd on the two Sm isotopes measured for internal normalization, i.e., ^{144}Sm and ^{148}Sm. ^{145}Nd was monitored and used to correct for Nd isobaric interferences during our stable Ce isotope measurements.

Two different correction methods for Nd isobaric interferences were compared. The first method ignores instrumental mass bias and directly subtracts Nd interferences from ^{142}Ce, ^{144}Sm, and ^{148}Sm intensities using the measured ^{145}Nd intensity and the average abundance of Nd isotopes in nature:

$$I_{^{142}Ce}^{corr} = I_{^{142}Ce}^{meas} - I_{^{145}Nd}^{meas} \times \left(\frac{^{142}Nd}{^{145}Nd}\right)_{true} \quad (4)$$

$$I_{^{144}Sm}^{corr} = I_{^{144}Sm}^{meas} - I_{^{145}Nd}^{meas} \times \left(\frac{^{144}Nd}{^{145}Nd}\right)_{true} \quad (5)$$

$$I_{^{148}Sm}^{corr} = I_{^{148}Sm}^{meas} - I_{^{145}Nd}^{meas} \times \left(\frac{^{148}Nd}{^{145}Nd}\right)_{true} \quad (6)$$

where ***I*** represents ion intensity, ***meas*** indicates the measured intensity, ***corr*** denotes the interference-corrected intensity, and ***true*** signifies the average natural Nd isotope ratio (i.e., ^{142}Nd/^{145}Nd = 3.2771, ^{144}Nd/^{145}Nd = 2.8675, and ^{148}Nd/^{145}Nd = 0.6867)[68].

The second method considers instrumental mass bias during interference correction, using ^{148}Sm/^{144}Sm and an iterative calculation. Mass bias factor (f) is first calculated using the measured ^{148}Sm/^{144}Sm ratio:

$$f = \frac{\ln\left(\frac{\left(^{148}Sm/^{144}Sm\right)_{true}}{\left(I_{meas}^{148}/I_{meas}^{144}\right)}\right)}{\ln\left(\frac{m^{148}Sm}{m^{144}Sm}\right)} \quad (7)$$

where $\boldsymbol{I_{meas}}$ indicates the measured ion intensity at mass 144 or 148, m represents atomic mass, and $\left(^{148}Sm/^{144}Sm\right)_{true}$ is 3.6612[68]. Assuming the same mass bias factor f applies to Nd isotopes, Nd interferences on Sm isotopes can be subtracted as follows:

$$I_{corr}^{144} = I_{meas}^{144} - I_{meas}^{^{145}Nd} \times \left(\frac{^{144}Nd}{^{145}Nd}\right)_{true} \times \left(\frac{m^{144}Nd}{m^{145}Nd}\right)^{f} \quad (8)$$

$$I_{corr}^{148} = I_{meas}^{148} - I_{meas}^{^{145}Nd} \times \left(\frac{^{148}Nd}{^{145}Nd}\right)_{true} \times \left(\frac{m^{148}Nd}{m^{145}Nd}\right)^{f} \quad (9)$$

Then, a $I_{corr}^{148}/I_{corr}^{144}$ ratio can be calculated and inserted back in Eq. 7 to replace $I_{meas}^{148}/I_{meas}^{144}$. Consequently, a new mass bias factor f can be calculated. The mass bias factor ***f*** typically converges after 10 iterations, and the calculated ***f*** no longer changes with more iterations, so we used 10 iterations in this study. The final ***f*** value is then used to correct for ^{142}Nd on ^{142}Ce, and, ultimately, stable Ce isotopes as follows:

$$I_{corr}^{142} = I_{meas}^{142} - I_{meas}^{^{145}Nd} \times \left(\frac{^{142}Nd}{^{145}Nd}\right)_{true} \times \left(\frac{m^{142}Nd}{m^{145}Nd}\right)^{f} \quad (10)$$

$$\left(^{142}Ce/^{140}Ce\right)_{corr} = \left(I_{corr}^{142}/I_{meas}^{^{140}Ce}\right) \times \left(\frac{m^{142}Ce}{m^{140}Ce}\right)^{f} \quad (11)$$

We conducted doping experiments to test the robustness of the two interference correction methods. NIST 3110 Ce solutions doped with different amount of Nd were analyzed on MC-ICP-MS, and data were corrected online during analysis using the two different correction methods. The results show that our iteration method allows for correction of a ~2 times higher level of ^{142}Nd interference compared to the correction that does not consider mass bias (Fig. 5). Considering a long-term precision of 0.04‰ (2SD) in ^{142}Ce/^{140}Ce in our laboratory, this iterative correction method allows for reliable isobaric correction at Nd/Ce mass ratios of up to ~10^{-3}, which is much higher than typical Nd/Ce mass ratios of geological rock samples after purification by our chromatographic separation method (<3×10^{-4}).

Stable Nd isotope measurements can be affected by various Sm isotopes (i.e., ^{144}Sm on ^{144}Nd, ^{148}Sm on ^{148}Nd, and ^{150}Sm on ^{150}Nd). ^{147}Sm was measured during our Nd isotope analysis to monitor and correct for isobaric interferences of Sm isotopes on relevant Nd isotopes. A mass bias factor was first calculated based on the measured ^{153}Eu/^{151}Eu and an assumed true value of 1.0916[68], and this mass bias factor was then applied to correct for isobaric interferences of Sm isotopes on Nd isotopes. For radiogenic ^{143}Nd/^{144}Nd ratio

measurements, interferences of Sm isotopes were corrected using an iterative calculation method similar to that described above for our stable Ce isotope analysis but based on $^{146}Nd/^{144}Nd$. Our correction methods significantly improved the robustness of our stable and radiogenic Nd isotope analysis (ESI Fig. S10). Although the iterative correction was previously used for radiogenic Nd isotope analysis[87], to the best of our knowledge, it has yet been widely applied to stable Ce and Nd isotope analysis on MC-ICP-MS in the community. Our results show evident analytical benefits that support the implementation of this approach during routine measurements of stable Ce and Nd isotopes.

3.2.3 Assessment of the dopant/analyte ratio mismatch on stable Ce and Nd isotope analysis

Because Sm (or Eu) was added to both samples and the bracketing standard during Ce (or Nd) isotope analysis, it is necessary to evaluate influence of the dopant/analyte ratio mismatch on the analysis. It was observed previously that instrumental mass bias was sensitive to the elemental dopant/analyte ratio during stable Cu and Zn isotope analysis[88], thereby making it essential to strictly match dopant/analyte ratios between the samples and bracketing standards. In contrast, a recent study found that stable Eu isotope ratios ($^{153}Eu/^{151}Eu$) measured on MC-ICP-MS remained constant within a large range of Sm-dopant to Eu ratios ($^{151}Eu/^{147}Sm$) between 0.2 and 5[89], making strict matching of the dopant/analyte ratio unnecessary. A recent study recommended that the concentration of the dopant element between the sample and bracketing standard should be kept within <10% for high-precision stable Nd isotope measurements[83], but the influence of dopant/analyte ratio mismatch on stable Ce isotope measurements has not been evaluated.

In our study, aliquots of NIST 3110 Ce solution were prepared to have the same Ce concentration (i.e., 100 ng/mL) but different Sm concentrations to yield Sm/Ce mass ratios between 1 and 3. These solutions were then analyzed against the same 100 ng/mL NIST 3110 Ce with 200 ng/mL Sm (Sm/Ce = 2) as the bracketing standard. No resolvable bias in measured $^{142}Ce/^{140}Ce$ ratios was observed (Fig. 6A). Our results demonstrate that stable Ce isotope measurement on our MC-ICP-MS instrument is not sensitive to ±50% mismatch of

Sm/Ce mass ratios between the sample and the bracketing standard. A Sm/Ce mass ratio of ~2 was typically adopted during our routine stable Ce isotope analysis.

Influence of the Eu/Nd doping ratio on stable Nd isotope analysis was assessed using a similar approach. Aliquots of 50 ng/mL JNdi-1 solution doped with 12.5 ng/mL, 18.75 ng/mL, 31.25 ng/mL and 37.5 ng/mL Eu were prepared and analyzed against the same 50 ng/mL JNdi-1 with 25 ng/mL Eu (Eu/Nd = 0.5). Similarly, no resolvable difference in measured Nd stable isotope ratios was observed within a range between +50% and -50% mismatch in Eu/Nd mass ratios between the sample and the bracketing standard (Fig. 6B). An Eu/Nd mass ratio of ~0.5 was typically adopted during our routine Nd isotope analysis.

3.3 Assessment of various forms of matrix effects on stable Ce and Nd isotope analysis

3.3.1 Concentration mismatch effect

Influence of analyte concentration mismatch between the sample and the bracketing standard was assessed by measurements of NIST 3110 Ce (or JNdi-1) solutions intentionally prepared to have Ce (or Nd) concentrations up to 50% more or less relative to the concentration used for the bracketing standard. Dopant/analyte ratios (Sm/Ce = 2 and Eu/Nd = 0.5) were kept the same between the sample and bracketing standard during stable Ce and Nd isotope measurement. Unlike strong concentration effects observed previously during stable K isotope analysis on "Sapphire" MC-ICP-MS using the low-energy collision cell path[90], stable Ce and Nd isotope measurements by the high-energy ion path of this instrument are not sensitive to even large concentration differences (i.e., 50%) between samples and bracketing standards (Fig. 7). The same method was applied to assess possible concentration effect during every analytical session in our laboratory over the entire course of this study, and it always showed negligible influence on stable Ce and Nd isotope measurements. Our results show that stringent concentration matching is not necessary; we typically matched sample-standard concentrations within ~5% as a precaution, although even larger

concentration mismatch would not influence the measurement based on our test results (Fig. 7). Correction was not needed at this level of concentration mismatch.

3.3.2 Acid concentrations

Previous studies have demonstrated that mismatch in the concentration of acid media that were used to dissolve samples and bracketing standards can bias stable isotopic analyses of a range of elements, for example, Fe[91, 92] and Mg[93, 94]. We evaluated this effect during stable Ce and Nd isotope analysis. NIST3110 Ce or JNdi-1 standard was prepared in HNO_3 of different concentrations ranging from 0.5% to 5% (v/v). These solutions were then analyzed against the same material prepared in 2% HNO_3. No measurable bias in the measured $\delta^{142}Ce$ was observed within our long-term precision of 0.04 ‰ (2SD) (Fig. 8A), whereas higher HNO_3 concentrations ($\geq$3%) led to measurably lower $\delta^{146}Nd$ relative to the true value (Fig. 8B). In our lab, we typically use the same batch of 2% HNO_3 to prepare both samples and bracketing standards during each session of stable Ce and Nd isotope measurements to avoid possible influence of acid concentration effects.

3.3.3 Matrix effects from inorganic cations

Matrix effects from common cations were assessed by analyzing a suite of NIST 3110 Ce or JNdi-1 solutions doped with varying amounts of cations against unadulterated NIST 3110 Ce or JNdi-1 solution. Cation impurities were added using high-purity single element standards. Eleven cations were tested, including common major or trace elements in geological samples (Na, Mg, Al, Fe, Ba), elements that may form oxide interferences (e.g., Te oxide on Ce), REEs neighboring or heavier than Ce and Nd (La, Pr, Gd, Ho, Lu).

Our test results show that all cations tested introduce little effect to stable Ce isotope analysis at [matrix cation]/[Ce] mass ratios of up to at least 10%, except for Al (Fig. 9A). The same tests were repeated for several cations in 2022 and 2023, and most results reproduced well. As a result, average results were plotted in Fig. 9A for cations that were tested in two different years. The absence of noticeable matrix effects from

Te indicates negligible formation of oxide interferences (i.e., $^{124}Te^{16}O^{+}$ on ^{140}Ce, $^{126}Te^{16}O^{+}$ on ^{142}Ce). A lack of perceptible matrix effects from La and Pr indicates little formation of hydride interferences (i.e., $^{139}La^{1}H^{+}$ on ^{140}Ce, $^{141}Pr^{1}H^{+}$ on ^{142}Ce) under dry plasma conditions. Similarly, most cations tested in this study produced negligible matrix effects at [matrix cation]/[Nd] mass ratios of up to at least 10% during stable Nd isotope analysis (Fig. 9B). It is particularly advantageous that the measured stable Nd isotope ratios are not influenced by the presence of Pr up to [Pr]/[Nd] mass ratios of 100% (ESI Fig. S11). Because elution peaks of Nd and Pr on the α-HIBA chromatographic column are very close (Fig. 1B), a larger volume that extends slightly into the Pr peak can be collected to ensure a more consistent high yield for Nd, without compromising Nd isotope measurements.

Among all the cations tested, Al is the only one that can cause biased stable Ce and Nd isotope measurements even at a moderate [Al]/[Ce (or Nd)] level of 2%. Unlike repeated tests of several other cations that yielded consistent results, the test performed in 2022 revealed a major impact on stable Ce isotope analysis from Al, whereas the test conducted in 2023 showed a negligible impact (Fig. 9A). This demonstrates that Al-induced matrix effects have highly variable influence on stable Ce isotope analysis. Our results showed that sufficient removal of Al ([Al]/[Ce (or Nd)] < 1%) via column separation is critical to ensure accurate stable Ce and Nd isotope analyses. Aluminum can be separated from bulk REEs during our 1st-stage chromatographic separation (Fig. 1A), and accurate stable Ce and Nd isotope results for a range of natural rock standards (Fig. 11) demonstrate effective removal of Al by our chromatographic procedure.

3.3.4 Matrix effects from organic α-HIBA compounds

Because α-HIBA can be left in the final Ce or Nd cut after the second-stage chromatographic separation, it is important to evaluate if residual α-HIBA can affect stable Ce and Nd isotope analysis. For Ce, aliquots of NIST 3110 Ce solutions were first mixed with different amounts of α-HIBA solution, and mixtures were then evaporated to complete dryness on a hotplate – a process mimicking how real samples are normally

processed before isotopic analysis. Finally, these test samples were redissolved in 2% HNO_3 and measured against pure NIST 3110 Ce on MC-ICP-MS. For comparison, two additional test samples were prepared by mixing 500 ng NIST 3110 Ce with 1.35 mmol α-HIBA, and then processed through the third-stage chromatographic column to remove all α-HIBA, followed by analysis on MC-ICP-MS. Our results show that the presence of α-HIBA can substantially affect stable Ce isotope analysis on our MC-ICP-MS (Fig. 10A). Recent studies on stable Eu isotope analysis showed that concentrated HNO_3 could decompose residual α-HIBA found in the Eu fraction from the α-HIBA chemistry so that accurate stable Eu isotope measurement could be achieved without an additional clean-up column[70, 95]. We tested this approach and found it ineffective for stable Ce isotope analysis; a ~0.1‰ bias in δ^{142}Ce could still be observed after a HNO_3 treatment (Fig. 10A). In contrast, our third-stage chromatographic column can effectively remove α-HIBA, and, hence, it is essential for accurate stable Ce isotope measurements (Fig. 10A).

Similar tests were also conducted for Nd. Although it is known that the presence of α-HIBA does not affect analysis of radiogenic $^{143}Nd/^{144}Nd$ ratios on MC-ICP-MS[96], our results clearly show that α-HIBA can produce matrix effects hampering accurate stable Nd isotope measurement (Fig. 10B). Again, this issue can be solved by the third-stage clean-up column that we developed.

3.4 Data accuracy and long-term precision of our new method

Accuracy and long-term precisions of our new method were assessed by routine analysis of geological reference materials and a series of pure standard solutions over a duration of more than 1 year. Nine different geological reference materials with a wide range of matrix composition were processed using our new three-step chromatographic procedure and then analyzed for their stable Ce and Nd isotopes, and radiogenic $^{143}Nd/^{144}Nd$ ratios on "Sapphire" MC-ICP-MS in our laboratory. In-house pure Ce solutions, namely UMN Ce-I, UMN Ce-II, and UMN Ce-III, were analyzed for their stable Ce isotopes with and without chromatographic separation, and no difference was observed. JNdi-1 was analyzed for radiogenic Nd isotope, and in-house pure Nd standards, Ames-I and Ames-II, were measured for both radiogenic and

stable Nd isotopes. Our results, together with published data for the same materials, if available, are compiled in ESI Table S4 and S5.

Our results of geological reference materials agreed well with published values (Fig. 11 and 12), demonstrating the accuracy of our new method. $^{143}Nd/^{144}Nd$ ratio of JMn-1 was never reported in literature, and we obtained a value of 0.512359 ± 0.000008 (2SD, n=8) for this material for the first time. Based on the results shown in Fig. 11 and 12, our long-term precision (2SD) is estimated to be ≤0.04‰ for $\delta^{142}Ce$, ≤0.03‰ for $\delta^{146}Nd$, and ≤15 ppm (i.e., 0.29 ε-unit) for radiogenic $^{143}Nd/^{144}Nd$ ratios.

It is important to note that several geological reference materials (BCR-2, BHVO-2, AGV-2/2a, GSP-2, JMn-1, NOD-P-1, NOD-A-1) have been analyzed for their stable Ce and Nd isotopes by multiple laboratories using different chromatographic methods and instruments, and interlaboratory results currently agree within a level of ≤0.066‰ for $\delta^{142}Ce$ and ≤0.034‰ for $\delta^{146}Nd$ for these reference materials (ESI Table S4 and S5). The interlaboratory agreement of $\delta^{146}Nd$ data for different reference materials is similar to the typical precision reported by individual laboratories (i.e., ~0.03‰), suggesting homogeneity of stable Nd isotopes in the suite of geological reference materials compiled here. However, the interlaboratory agreement of $\delta^{142}Ce$ varies for different reference materials, ranging from 0.020‰ for NOD-A-1 to 0.066‰ for BCR-2. The level of agreement is often larger than the reported precisions for $\delta^{142}Ce$ in individual laboratories (~0.04‰), reflecting either true heterogeneity of stable Ce isotopes in some reference materials considered here (e.g., BCR-2) or subtle analytical artefacts associated with different methods used in different laboratories. Further interlaboratory comparison of stable Ce isotope analysis is needed and beneficial for further stable Ce isotope research, in particular, study of high-temperature processes where stable Ce isotope variations are expected to be small.

Conclusions

A new and robust chromatographic procedure was developed and demonstrated to be able to simultaneously separate Ce and Nd from geological materials of a wide range of matrix composition for high-precision analysis of stable Ce and Nd isotopes, and radiogenic $^{143}Nd/^{144}Nd$ ratios. The elution protocol for the α-HIBA column, the key stage of sequential Nd and Ce separation, was optimized, and column-induced stable Ce and Nd isotope fractionation was also quantified. An iterative method was developed to correct for possible isobaric interferences (i.e., ^{142}Nd on ^{142}Ce and ^{144}Sm on ^{144}Nd) during stable Ce and Nd isotope analysis, and this correction method can improve the robustness of our measurements. Various forms of matrix effects, including dopant/analyte ratios, concentration mismatch in acid media and between the sample and the bracketing standard, presence of common inorganic cations and residual α-HIBA, were systematically evaluated for stable Ce and Nd isotope analysis on MC-ICP-MS ("Sapphire", Nu Instruments) under dry plasma conditions. Routine analyses of 9 different geological reference materials and several high-purity standard solutions over more than 1 year yielded accurate stable Ce and Nd isotope results, with demonstrated long-term precision (2SD) of better than 0.04‰ for $\delta^{142}Ce$ and better than 0.03‰ for $\delta^{146}Nd$. Our new chromatographic method is also applicable to preparation of geological samples for accurate analysis of radiogenic $^{143}Nd/^{144}Nd$ ratios, and a long-term precision (2SD) of better than 15ppm (i.e., 0.29 ε-unit) was achieved in our laboratory. Our results also show the potential of α-HIBA chemistry for separation of other REEs beyond Ce and Nd for their stable and radiogenic isotope measurements.

Acknowledgement

This work is supported by the US National Science Foundation under Grant No. 2049554 to X.-Y. Zheng.

Figure captions

Fig. 1 Elution curves for the first-stage (A), second-stage (B), and third-stage (C) chromatographic column. Note that Nd is processed the same way as shown for Ce during the third-stage column. The shaded areas represent volumes collected for Ce and Nd.

Fig. 2 A elution comparison between single 0.225 M α-HIBA solution and combined 0.150 M + 0.225 M α-HIBA solutions. (A) Percentage of Nd collected in the Nd cut (2.4 mL), Ce cut (6 mL), and 3 pre-cuts (0.4 mL each) and 3 post-cuts (0.4 mL each) before and after Nd and Ce collection using only 0.225 M α-HIBA solution as the eluent. Pure multi-REEs solution shows quantitative recovery of Nd in the Nd cut, negligible tailing and good separation between Nd and Ce. However, substantial tailing of Nd into the Ce cut is observed for rock samples (BCR-2, AGV-2a, BHVO-2). (B) Percentage of Nd collected in the Nd cut, Ce cut, and 3 pre- and post-cuts for each using combined 0.150 M + 0.225 M α-HIBA solutions as the eluents. Good separation and more consistent elution profiles can be observed regardless of sample matrices. (C) Sm/Nd mass ratios and Nd/Ce mass ratios in the original samples (diamonds) and the purified Nd and Ce cuts after the α-HIBA column using different elution protocols (0.225 M α-HIBA: squares; 0.150 M + 0.225 M α-HIBA: circles). For the pure multi-REEs solution, similar Sm/Nd and Nd/Ce ratios were obtained using either of the two elution protocols tested here. In contrast, for geological materials, elution by a combined use of 0.150 M and 0.225 M α-HIBA resulted in significantly better purification of Nd and Ce.

Fig. 3 Stable Ce isotopes ($^{142}Ce/^{140}Ce$) (A) and stable Nd isotopes ($^{146}Nd/^{144}Nd$) (B) in different fractions plotted against the accumulative weight fraction in a probability scale. The horizontal line on each data symbol in both plots indicates the range of the accumulative Ce (or Nd) weight fraction each measured sample represents. Data are plotted at the median point of the accumulative weight fraction in each fraction, and all data from the same experiments were fitted by linear regression to estimate isotope fractionation factors induced by the column separation.

Fig. 4 A comparison of data quality associated with simple SSB (squares) and C-SSBIN (circles) mass bias correction methods for δ^{142}Ce (A) and δ^{146}Nd (B). Each data point represents one individual measurement that includes at least 3 repeated analyses of the same solution. Use of a C-SSBIN method clearly results in better precision for both stable Ce and Nd isotope measurements compared to use of a simple SSB method.

Fig. 5 A comparison of two different correction methods for ^{142}Nd interferences on ^{142}Ce during stable Ce isotope measurements. The shaded bar indicates the true δ^{142}Ce value (0‰) of the measured NIST Ce solution with our typical precision of 0.04‰ (2SD). Blue squares represent the corrected δ^{142}Ce data based on average natural abundances of different Nd isotopes without considering instrumental mass bias. Orange circles show the corrected δ^{142}Ce data after 1 iterative correction, and purple diamonds show the results corrected by >10-time iterative corrections. Orange arrow suggests that the value after 1 iterative correction is lower than -15‰. Our iterative method allows for reliable isobaric interference correction at a Nd/Ce ratio of ~2-time higher compared to that permissible by the simple correction method ignoring instrumental mass bias.

Fig. 6 Influence of variable dopant/analyte ratios on δ^{142}Ce (A) and δ^{146}Nd (B). The shaded bar in both plots indicates the true δ-value with our typical long-term precision. Yellow stars denote the Sm or Eu concentration used in the bracketing standards.

Fig. 7 Influence of analyte concentration mismatch on δ^{142}Ce (A) and δ^{146}Nd (B). Samples and bracketing standards have the same dopant/analyte ratios. The shaded bar indicates the true δ-value with our typical long-term precision. Yellow stars denote the bracketing standard.

Fig. 8 Influence of acid concentrations on δ^{142}Ce (A) and δ^{146}Nd (B). The same tests for stable Ce isotope measurements were conducted in the Year 2022 (blue circles) and Year 2023 (green squares). The shaded bar indicates the true δ-value with our typical long-term precision. Yellow stars denote the bracketing standard.

Fig. 9 (A) Matrix effects of common inorganic cations on δ^{142}Ce. Elements labeled with "_A" denotes average data from two independent tests conducted in the Year 2022 and 2023, which yielded similar values. δ^{142}Ce data with Al doping from two years are plotted separately because they exhibit different behaviors. (B) Matrix effects of inorganic cations on δ^{146}Nd. The shaded bar indicates the true δ-value with our typical long-term precision.

Fig. 10 (A) Matrix effects of α-HIBA on δ^{142}Ce. Green circles represent data measured after sample purification by the third-stage chromatographic chemistry to remove α-HIBA. Orange diamonds indicate samples that were treated with concentrated HNO_3 to decompose α-HIBA. Light and dark blue points are samples with different Ce to α-HIBA mixing ratios. (B) Matrix effects of α-HIBA on δ^{146}Nd. In both cases, the measured δ^{142}Ce and δ^{146}Nd were biased in the presence of α-HIBA. The shaded bar indicates the true δ-value with our typical long-term precision.

Fig. 11 $\delta^{142}Ce_{NIST\ 3110}$ results (A) and $\delta^{146}Nd_{JNdi\text{-}1}$ results (B) of reference materials in this study plotted against literature data. The error bar represents 2SD. All data are compiled in ESI Table S4 and S5.

Fig. 12 Radiogenic $^{143}Nd/^{144}Nd$ ratios obtained in this study in comparison to literature data. The error bar represents 2SD. All data are compiled in ESI Table S5.

References

1. A. Pourmand, N. Dauphas and T. J. Ireland, *Chem Geol*, 2012, **291**, 38-54.
2. P. Henderson, *Rare earth element geochemistry*, Elsevier, 2013.
3. S. M. McLennan and S. Ross Taylor, in *Encyclopedia of Inorganic and Bioinorganic Chemistry*, DOI: https://doi.org/10.1002/9781119951438.eibc2004.
4. C. R. German and H. Elderfield, *Paleoceanography*, 1990, **5**, 823-833.
5. C. R. German, B. P. Holliday and H. Elderfield, *Geochimica Et Cosmochimica Acta*, 1991, **55**, 3553-3558.
6. J. A. Barrat, G. Bayon and S. Lalonde, *Chem Geol*, 2023, **615**, 121202.
7. X. M. Liu, L. C. Kah, A. H. Knoll, H. Cui, C. Wang, A. Bekker and R. M. Hazen, *Nat Commun*, 2021, **12**, 351.
8. R. Tostevin, R. A. Wood, G. A. Shields, S. W. Poulton, R. Guilbaud, F. Bowyer, A. M. Penny, T. He, A. Curtis, K. H. Hoffmann and M. O. Clarkson, *Nat Commun*, 2016, **7**, 12818.
9. K. Zhang and G. A. Shields, *Earth Sci Rev*, 2022, **229**, 104015.
10. K. Zhang, X. K. Zhu, R. A. Wood, Y. Shi, Z. F. Gao and S. W. Poulton, *Nat Geosci*, 2018, **11**, 345-350.
11. A. Makishima, E. Nakamura, S.-i. Akimoto, I. H. Campbell and R. I. Hill, *Chem Geol*, 1993, **104**, 293-300.
12. F. Meissner, W. Schmidt-Ott and L. Ziegeler, *Z. Phys. A: At. Nucl.;(Germany, Federal Republic of)*, 1987, **327**.
13. L. Fang, P. Frossard, M. Boyet, A. Bouvier, J. A. Barrat, M. Chaussidon and F. Moynier, *Proceedings of the National Academy of Sciences*, 2022, **119**, e2120933119.
14. G. Lugmair and K. Marti, *Earth Planet Sci Lett*, 1978, **39**, 349-357.
15. T. Tanaka and A. Masuda, *Nature*, 1982, **300**, 515-518.
16. A. P. Dickin, *Nature*, 1987, **325**, 337-338.
17. P. Bonnand, S. V. Lalonde, M. Boyet, C. Heubeck, M. Homann, P. Nonnotte, I. Foster, K. O. Konhauser and I. Köhler, *Earth Planet Sci Lett*, 2020, **547**, 116452.
18. J. O. S. Santos, L. A. Hartmann, H. E. Gaudette, D. I. Groves, N. J. McNaughton and I. R. Fletcher, *Gondwana Research*, 2000, **3**, 453-488.
19. A. P. Dickin, *Nature*, 1987, **326**, 283-284.
20. T. Tanaka, H. Shimizu, Y. Kawata and A. Masuda, *Nature*, 1987, **327**, 113-117.
21. A. Makishima and A. Masuda, *Chem Geol*, 1994, **118**, 1-8.
22. H. Shimizu, H. Sawatari, Y. Kawata, P. N. Dunkley and A. Masuda, *CoMP*, 1992, **110**, 242-252.
23. H. Amakawa, J. Ingri, A. Masuda and H. Shimizu, *Earth Planet Sci Lett*, 1991, **105**, 554-565.
24. H. Shimizu, M. Amano and A. Masuda, *Geology*, 1991, **19**, 369-371.
25. N. Bellot, M. Boyet, R. Doucelance, C. Pin, C. Chauvel and D. Auclair, *Geochimica Et Cosmochimica Acta*, 2015, **168**, 261-279.
26. M. Boyet, R. Doucelance, C. Israel, P. Bonnand, D. Auclair, K. Suchorski and C. Bosq, *GGG*, 2019, **20**, 2484-2498.
27. F. Albarède and S. L. Goldstein, *Geology*, 1992, **20**, 761-763.
28. R. Doucelance, N. Bellot, M. Boyet, T. Hammouda and C. Bosq, *Earth Planet Sci Lett*, 2014, **407**, 175-186.
29. M. Tanaka, H. Shimizu, Y. Nozaki, Y. Ikeuchi and A. Masuda, *GeocJ*, 1990, **24**, 309-314.
30. H. Shimizu, K. Tachikawa, A. Masuda and Y. Nozaki, *Geochimica et Cosmochimica Acta*, 1994, **58**, 323-333.
31. F. Lacan, K. Tachikawa and C. Jeandel, *Chem Geol*, 2012, **300-301**, 177-184.
32. H. Shimizu, T. Tanaka and A. Masuda, *Nature*, 1984, **307**, 251-252.
33. A. Makishima and A. Masuda, *Chem Geol*, 1993, **106**, 197-205.
34. C. Israel, M. Boyet, R. Doucelance, P. Bonnand, P. Frossard, D. Auclair and A. Bouvier, *Earth Planet Sci Lett*, 2020, **530**, 115941.

35. R. W. Carlson, M. Boyet and M. Horan, *Science*, 2007, **316**, 1175-1178.
36. M. Boyet and R. W. Carlson, *Science*, 2005, **309**, 576-581.
37. W. S. Li, R. Nakada, Y. Takahashi, R. M. Gaschnig, Y. F. Hu, M. Shakouri, R. L. Rudnick and X. M. Liu, *Geochimica et Cosmochimica Acta*, 2023, **359**, 20-29.
38. R. Nakada, Y. Takahashi and M. Tanimizu, *Geochimica Et Cosmochimica Acta*, 2016, **181**, 89-100.
39. R. Nakada, Y. Takahashi and M. Tanimizu, *Geochimica Et Cosmochimica Acta*, 2013, **103**, 49-62.
40. R. Nakada, M. Tanaka, M. Tanimizu and Y. Takahashi, *Geochimica Et Cosmochimica Acta*, 2017, **218**, 273-290.
41. W. Li, X.-M. Liu, R. Nakada, Y. Takahashi, Y. Hu, M. Shakouri, Z. Zhang, T. Okumura and S. Yamada, *Earth Planet Sci Lett*, 2023, **602**, 117962.
42. W. W. Fischer, J. Hemp and J. E. Johnson, *Annual Review of Earth and Planetary Sciences*, 2016, **44**, 647-683.
43. W. Liu, J. Hao, E. J. Elzinga, P. Piotrowiak, V. Nanda, N. Yee and P. G. Falkowski, *Proceedings of the National Academy of Sciences*, 2020, **117**, 22698-22704.
44. A. J. McCoy-West, K. W. Burton, M. A. Millet and P. A. Cawood, *Geochimica et Cosmochimica Acta*, 2021, **293**, 575-597.
45. A. J. McCoy-West, M. A. Millet and K. W. Burton, *Earth Planet Sci Lett*, 2017, **480**, 121-132.
46. J. H. Bai, K. Luo, C. Wu, Z. B. Wang, L. Zhang, S. Yan, S. X. Zhong, J. L. Ma and G. J. Wei, *Earth Planet Sci Lett*, 2023, **617**, 118260.
47. X. Liu, G. J. Wei, J. Q. Zou, Y. R. Guo, J. L. Ma, X. F. Chen, Y. Liu, J. F. Chen, H. L. Li and T. Zeng, *Journal of Geophysical Research: Oceans*, 2018, **123**, 9137-9155.
48. A. J. McCoy-West, N. Mortimer, K. W. Burton, T. R. Ireland and P. A. Cawood, *Gondwana Research*, 2022, **105**, 432-449.
49. A. J. McCoy-West, M. A. Millet and K. W. Burton, *Frontiers in Earth Science*, 2020, **8**.
50. J. Y. Hu, N. Dauphas, F. L. H. Tissot, R. Yokochi, T. J. Ireland, Z. Zhang, A. M. Davis, F. J. Ciesla, L. Grossman, B. L. A. Charlier, M. Roskosz, E. E. Alp, M. Y. Hu and J. Zhao, *Sci Adv*, 2021, **7**, eabc2962.
51. T. Ohno and T. Hirata, *Anal Sci*, 2013, **29**, 47-53.
52. J. H. Bai, J. L. Ma, G. J. Wei, L. Zhang and S. X. Zhong, *JAAS*, 2022, **37**, 1618-1628.
53. J. Y. Hu, F. L. H. Tissot, R. Yokochi, T. J. Ireland, N. Dauphas and H. M. Williams, *ACS Earth and Space Chemistry*, 2023, **7**, 2222-2238.
54. G. R. Choppin and R. J. Silva, *Journal of Inorganic & Nuclear Chemistry*, 1956, **3**, 153-154.
55. H. L. Smith and D. C. Hoffman, *Journal of Inorganic & Nuclear Chemistry*, 1956, **3**, 243-247.
56. G. Lugmair, N. Scheinin and K. Marti, 1975.
57. D. J. Depaolo and G. J. Wasserburg, *Geophysical Research Letters*, 1976, **3**, 249-252.
58. S. B. Jacobsen and G. J. Wasserburg, *Earth Planet Sci Lett*, 1980, **50**, 139-155.
59. H. Shimizu, S. Nakai, S. Tasaki, A. Masuda, D. Bridgwater, A. P. Nutman and H. Baadsgaard, *Earth Planet Sci Lett*, 1988, **91**, 159-169.
60. N. E. Marks, L. E. Borg, I. D. Hutcheon, B. Jacobsen and R. N. Clayton, *Earth Planet Sci Lett*, 2014, **405**, 15-24.
61. E. Hyung and F. L. H. Tissot, *JAAS*, 2021, **36**, 1946-1959.
62. C. M. Johnson and R. A. Thompson, *Journal of Geophysical Research: Solid Earth*, 1991, **96**, 13593-13608.
63. A. M. Satkoski, P. Fralick, B. L. Beard and C. M. Johnson, *Geochimica et Cosmochimica Acta*, 2017, **209**, 216-232.
64. T. Tanaka, S. Togashi, H. Kamioka, H. Amakawa, H. Kagami, T. Hamamoto, M. Yuhara, Y. Orihashi, S. Yoneda, H. Shimizu, T. Kunimaru, K. Takahashi, T. Yanagi, T. Nakano, H. Fujimaki, R. Shinjo, Y. Asahara, M. Tanimizu and C. Dragusanu, *Chem Geol*, 2000, **168**, 279-281.

65. B. L. Beard, L. G. Medaris, C. M. Johnson, E. Jelinek, J. Tonika and L. R. Riciputi, *Geologische Rundschau*, 1995, **84**, 552-567.
66. A. Pourmand and N. Dauphas, *Talanta*, 2010, **81**, 741-753.
67. R. Nakada, N. Asakura and K. Nagaishi, *GeocJ*, 2019, **53**, 293-304.
68. J. R. de Laeter, J. K. Böhlke, P. De Bièvre, H. Hidaka, H. S. Peiser, K. J. R. Rosman and P. D. P. Taylor, *Pure and Applied Chemistry*, 2003, **75**, 683-800.
69. S. Wakaki and T. Tanaka, *International Journal of Mass Spectrometry*, 2012, **323-324**, 45-54.
70. S. G. Lee and T. Tanaka, *International Journal of Mass Spectrometry*, 2021, **469**, 116668.
71. F. Liu, M. X. Ling, Z. F. Zhang, W. N. Lu, J. B. Xu, X. Li, D. Yang, J. J. Wu and H. Yang, *Chem Geol*, 2023, **637**, 121664.
72. N. S. Saji, D. Wielandt, C. Paton and M. Bizzarro, *JAAS*, 2016, **31**, 1490-1504.
73. E. Glueckauf, *Transactions of the Faraday Society*, 1955, **51**, 34-44.
74. E. Glueckauf, *Transactions of the Faraday Society*, 1958, **54**, 1203-1205.
75. H. Li, F. L. H. Tissot, S.-G. Lee, E. Hyung and N. Dauphas, *ACS Earth and Space Chemistry*, 2020, **5**, 55-65.
76. F. Liu, Z. Zhang, X. Li, Y. An, Y. Liu, K. Chen, Z. Bao and C. Li, *Anal Chem*, 2021, **93**, 12524-12531.
77. F. Liu, X. Li, H. Yang, Q. Y. Peng, J. J. Wu and Z. F. Zhang, *JAAS*, 2023, DOI: 10.1039/d3ja00284e.
78. G. L. Arnold, S. Weyer and A. D. Anbar, *AnaCh*, 2004, **76**, 322-327.
79. X. K. Zhu, Y. Guo, R. K. O'Nions, E. D. Young and R. D. Ash, *Nature*, 2001, **412**, 311-313.
80. J. E. Roe, A. D. Anbar and J. Barling, *Chem Geol*, 2003, **195**, 69-85.
81. A. D. Anbar, K. A. Knab and J. Barling, *AnaCh*, 2001, **73**, 1425-1431.
82. H. Pourkhorsandi, V. Debaille, J. de Jong and R. M. G. Armytage, *Talanta*, 2021, **224**, 121877.
83. J. H. Bai, F. Liu, Z. F. Zhang, J. L. Ma, L. Zhang, Y. F. Liu, S. X. Zhong and G. J. Wei, *JAAS*, 2021, **36**, 2695-2703.
84. J. H. Bai, J. L. Ma, G. J. Wei, L. Zhang, C. S. Liu, T. Gao, Y. H. Liu and Y. F. Liu, *Geostandards and Geoanalytical Research*, 2022, **46**, 825-836.
85. J. L. Ma, G. J. Wei, Y. Liu, Z. Y. Ren, Y. G. Xu and Y. H. Yang, *JAAS*, 2013, **28**, 1926.
86. Y. Q. Wang, X. X. Huang, Y. L. Sun, S. Q. Zhao and Y. H. Yue, *Analytical Methods*, 2017, **9**, 3531-3540.
87. G. L. Foster and D. Vance, *JAAS*, 2006, **21**, 288.
88. C. Archer and D. Vance, *JAAS*, 2004, **19**, 656.
89. L. Nicol, M. Garçon, M. Boyet and A. Gannoun, *JAAS*, 2023, **38**, 1261-1274.
90. X. Y. Zheng, X. Y. Chen, W. M. Ding, Y. C. Zhang, S. Charin and Y. Gerard, *JAAS*, 2022, **37**, 1273-1287.
91. J. Wang, D. M. Tang, B. X. Su, Q. H. Yuan, W. J. Li, B. Y. Gao, K. Y. Chen, Z. A. Bao and Y. Zhao, *JAAS*, 2022, **37**, 1869-1875.
92. N. Dauphas, A. Pourmand and F.-Z. Teng, *Chem Geol*, 2009, **267**, 175-184.
93. J. K. Liu and G. L. Han, *JAAS*, 2021, **36**, 1986-1995.
94. F. Z. Teng and W. Yang, *Rapid Communications in Mass Spectrometry*, 2014, **28**, 19-24.
95. S. G. Lee and T. Tanaka, *Spectrochimica Acta Part B: Atomic Spectroscopy*, 2019, **156**, 42-50.
96. X. Y. Zheng, H. C. Jenkyns, A. S. Gale, D. J. Ward and G. M. Henderson, *Earth Planet Sci Lett*, 2013, **375**, 338-348.

Fig. 1

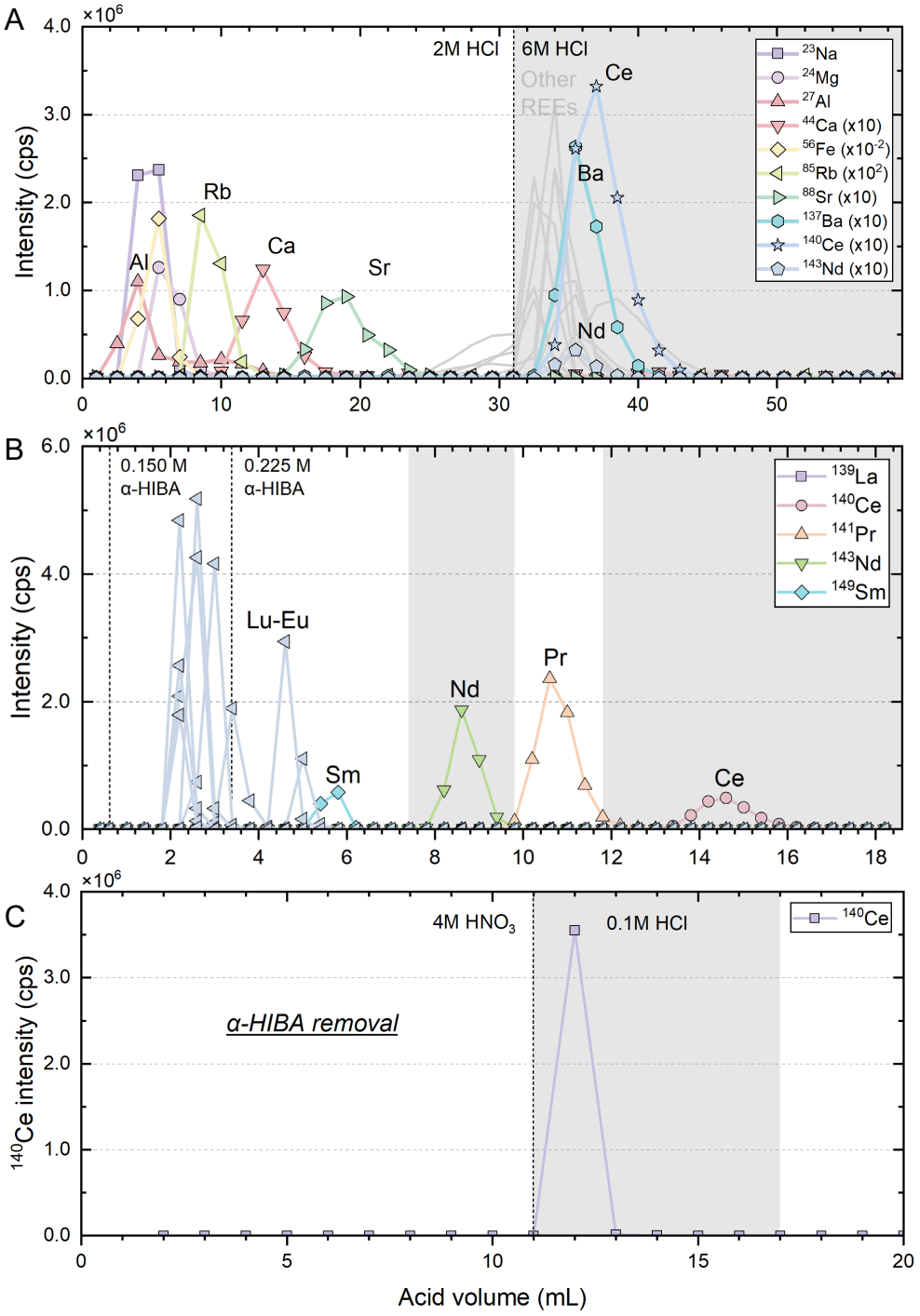
A
×10^6
Intensity (cps)
2M HCl
6M HCl
Other REEs
Ce
Ba
Rb
Ca
Sr
Al
Nd
23Na
24Mg
27Al
44Ca (x10)
56Fe (x10-2)
85Rb (x10^2)
88Sr (x10)
137Ba (x10)
140Ce (x10)
143Nd (x10)
B
×10^6
Intensity (cps)
0.150 M α-HIBA
0.225 M α-HIBA
Lu-Eu
Nd
Pr
Sm
Ce
139La
140Ce
141Pr
143Nd
149Sm
C
×10^6
140Ce intensity (cps)
4M HNO3
0.1M HCl
α-HIBA removal
140Ce
Acid volume (mL)

Fig. 2

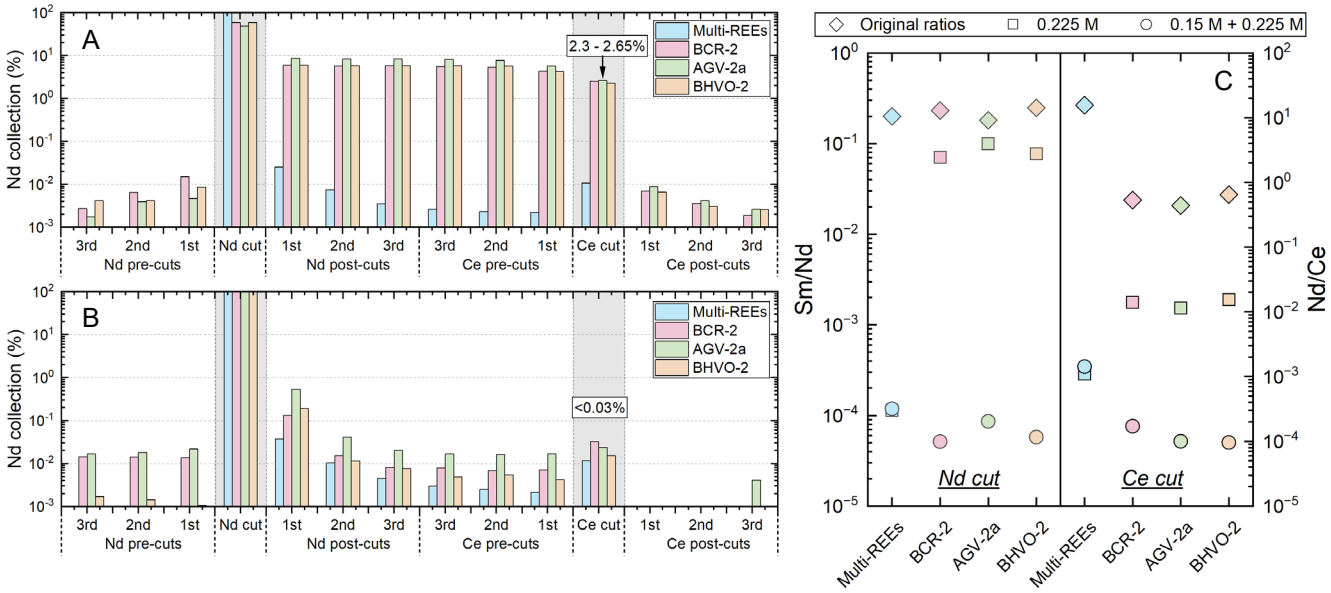
A
B
C
Nd collection (%)
Multi-REEs
BCR-2
AGV-2a
BHVO-2
2.3 - 2.65%
<0.03%
3rd 2nd 1st Nd pre-cuts
Nd cut
1st 2nd 3rd Nd post-cuts
3rd 2nd 1st Ce pre-cuts
Ce cut
1st 2nd 3rd Ce post-cuts
Original ratios
0.225 M
0.15 M + 0.225 M
Sm/Nd
Nd/Ce
Nd cut
Ce cut

Fig. 3

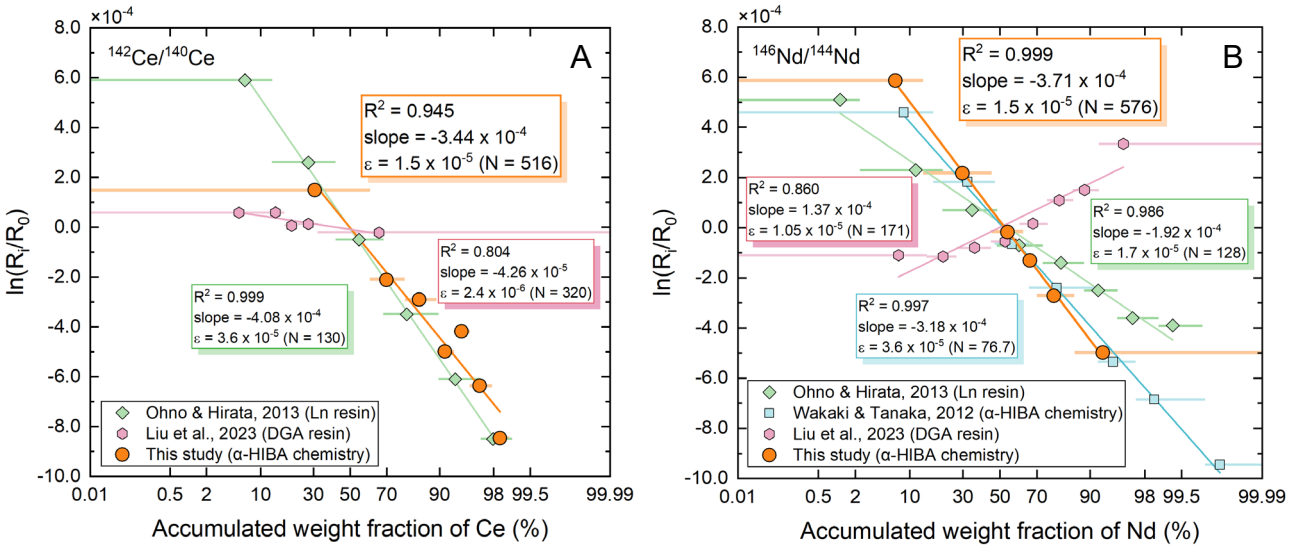
×10-4
142Ce/140Ce
A
R2 = 0.945
slope = -3.44 x 10-4
ε = 1.5 x 10-5 (N = 516)
R2 = 0.804
slope = -4.26 x 10-5
ε = 2.4 x 10-6 (N = 320)
R2 = 0.999
slope = -4.08 x 10-4
ε = 3.6 x 10-5 (N = 130)
Ohno & Hirata, 2013 (Ln resin)
Liu et al., 2023 (DGA resin)
This study (α-HIBA chemistry)
ln(Rf/R0)
Accumulated weight fraction of Ce (%)
146Nd/144Nd
B
R2 = 0.999
slope = -3.71 x 10-4
ε = 1.5 x 10-5 (N = 576)
R2 = 0.860
slope = 1.37 x 10-4
ε = 1.05 x 10-5 (N = 171)
R2 = 0.986
slope = -1.92 x 10-4
ε = 1.7 x 10-5 (N = 128)
R2 = 0.997
slope = -3.18 x 10-4
ε = 3.6 x 10-5 (N = 76.7)
Ohno & Hirata, 2013 (Ln resin)
Wakaki & Tanaka, 2012 (α-HIBA chemistry)
Liu et al., 2023 (DGA resin)
This study (α-HIBA chemistry)
Accumulated weight fraction of Nd (%)

Fig. 4

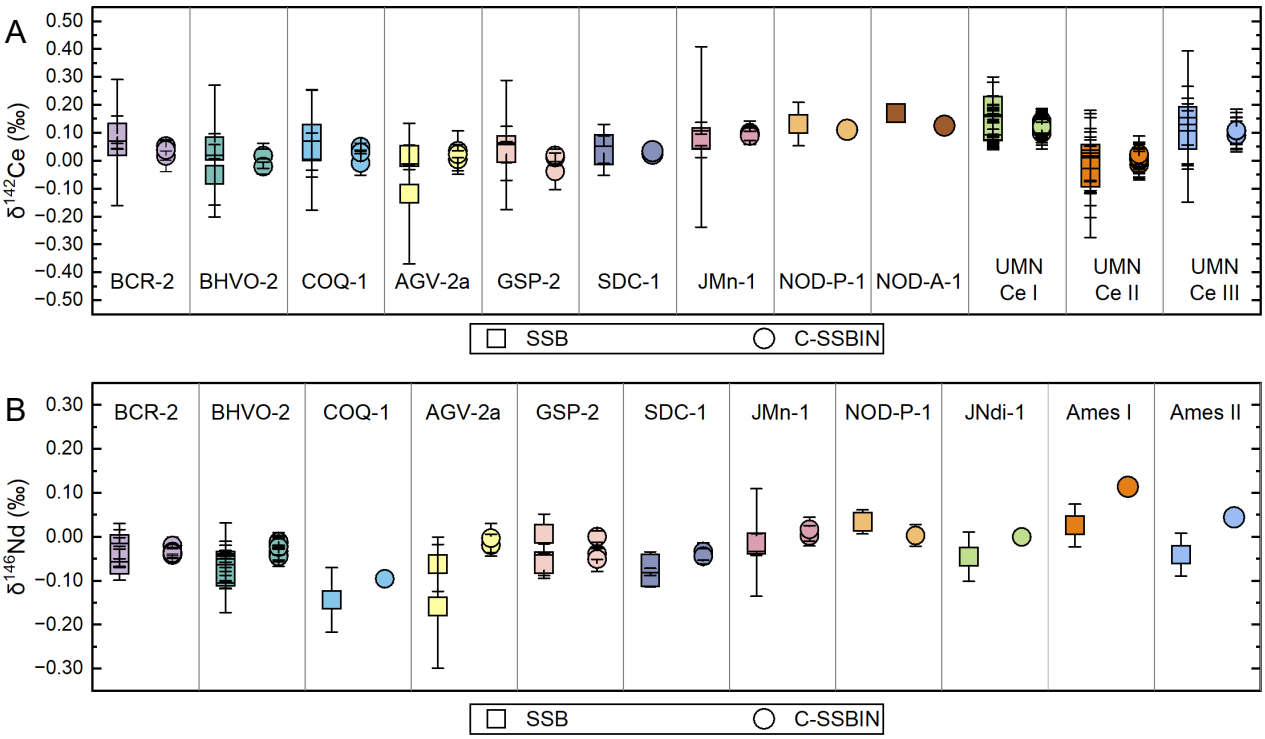
A
δ142Ce (‰)
0.50
0.40
0.30
0.20
0.10
0.00
−0.10
−0.20
−0.30
−0.40
−0.50
BCR-2
BHVO-2
COQ-1
AGV-2a
GSP-2
SDC-1
JMn-1
NOD-P-1
NOD-A-1
UMN Ce I
UMN Ce II
UMN Ce III
SSB
C-SSBIN
B
δ146Nd (‰)
0.30
0.20
0.10
0.00
−0.10
−0.20
−0.30
BCR-2
BHVO-2
COQ-1
AGV-2a
GSP-2
SDC-1
JMn-1
NOD-P-1
JNdi-1
Ames I
Ames II
SSB
C-SSBIN

Fig. 5

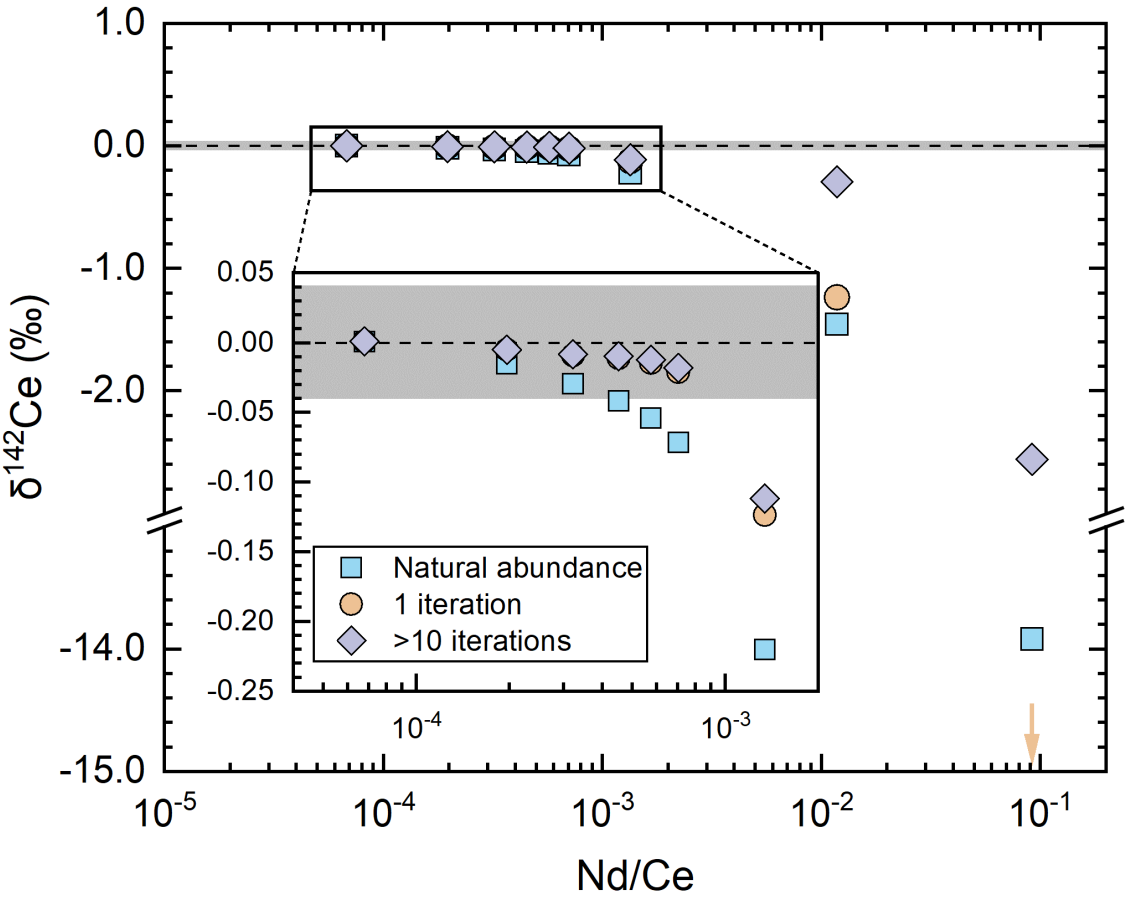
1.0
0.0
-1.0
-2.0
-14.0
-15.0
δ142Ce (‰)
0.05
0.00
-0.05
-0.10
-0.15
-0.20
-0.25
10-4
10-3
Natural abundance
1 iteration
>10 iterations
10-5
10-4
10-3
10-2
10-1
Nd/Ce

Fig. 6

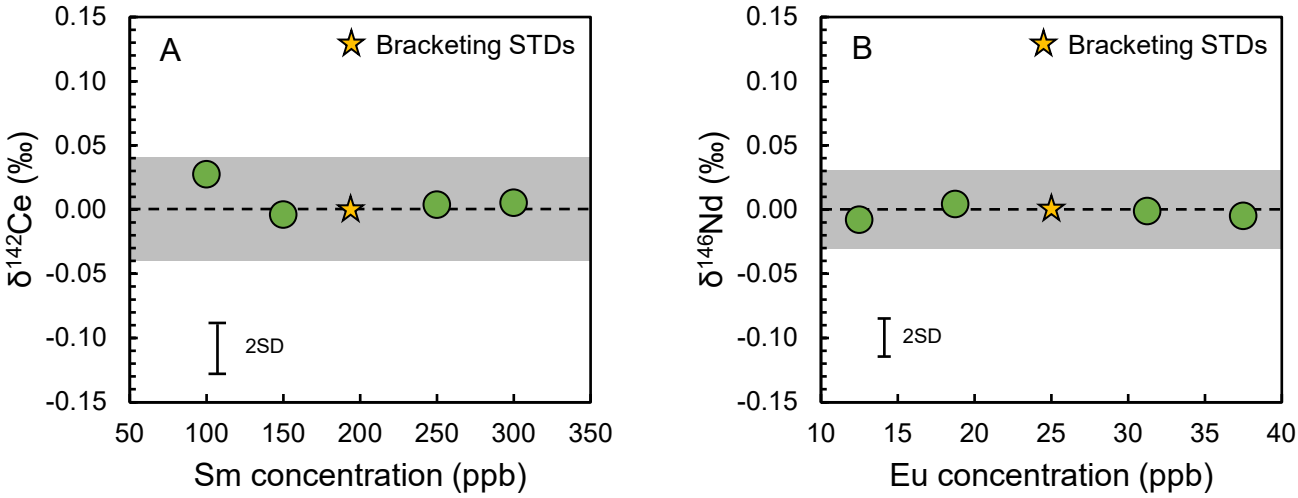
A
Bracketing STDs
2SD
δ142Ce (‰)
Sm concentration (ppb)
B
Bracketing STDs
2SD
δ146Nd (‰)
Eu concentration (ppb)

Fig. 7

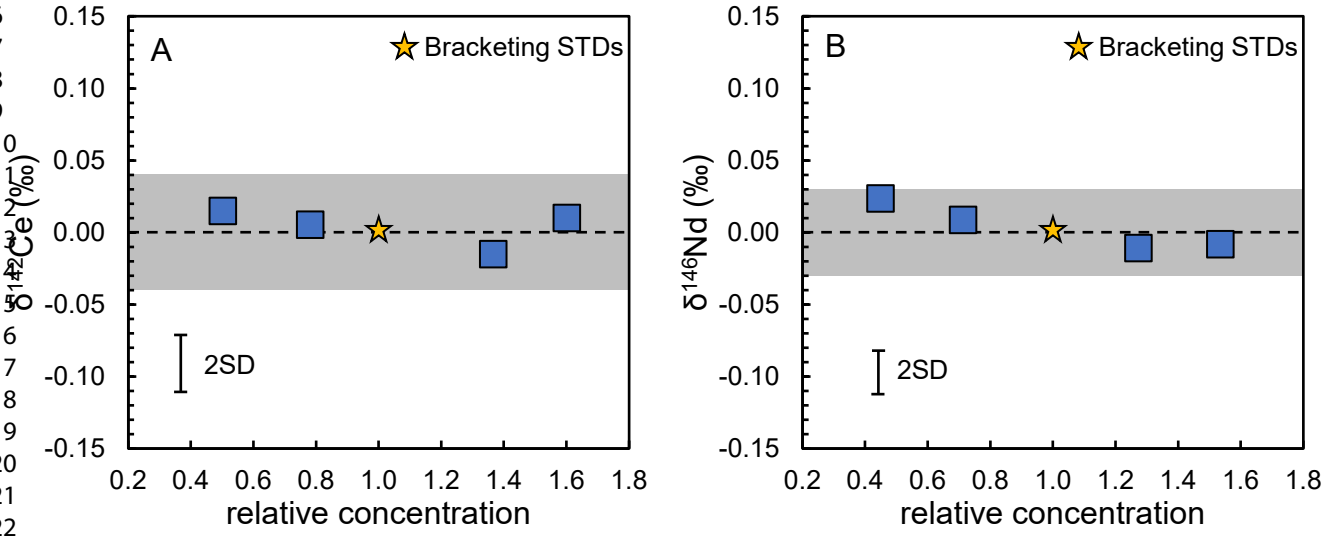
A
Bracketing STDs
2SD
δ142Ce (‰)
relative concentration
B
Bracketing STDs
2SD
δ146Nd (‰)
relative concentration

Fig. 8

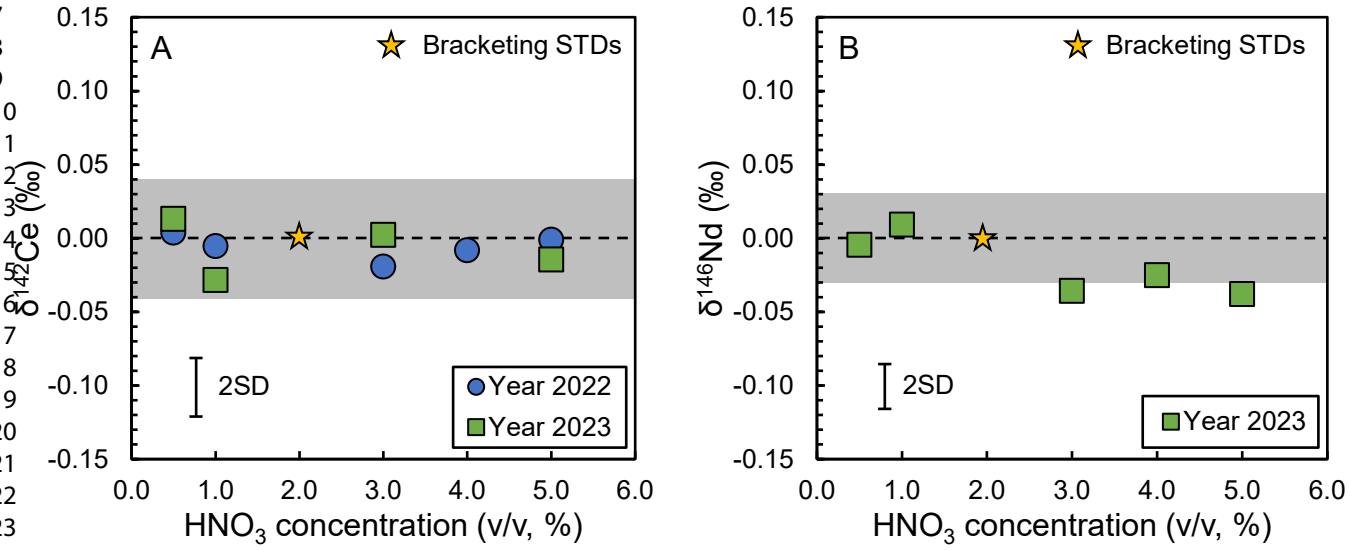
A
Bracketing STDs
2SD
Year 2022
Year 2023
δ142Ce (‰)
HNO3 concentration (v/v, %)
B
Bracketing STDs
2SD
Year 2023
δ146Nd (‰)
HNO3 concentration (v/v, %)

Fig. 9

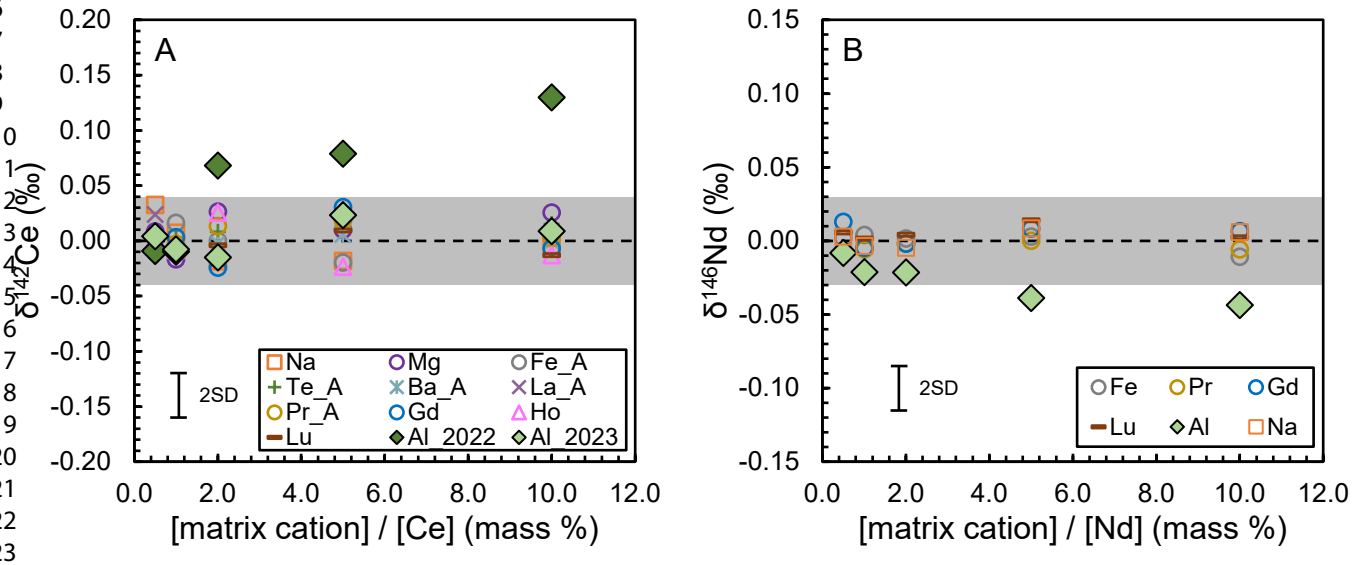
A
B
δ142Ce (‰)
δ146Nd (‰)
[matrix cation] / [Ce] (mass %)
[matrix cation] / [Nd] (mass %)
2SD
Na
Mg
Fe_A
Te_A
Ba_A
La_A
Pr_A
Gd
Ho
Lu
Al_2022
Al_2023
Fe
Pr
Gd
Lu
Al
Na

Fig. 10

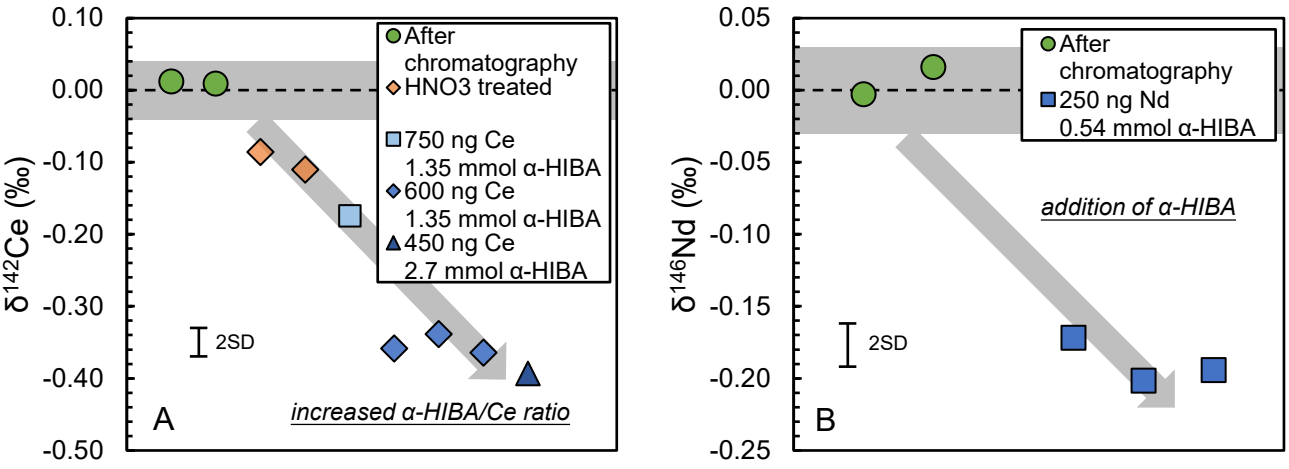
0.10
0.00
-0.10
-0.20
-0.30
-0.40
-0.50
δ142Ce (‰)
After chromatography
HNO3 treated
750 ng Ce
1.35 mmol α-HIBA
600 ng Ce
1.35 mmol α-HIBA
450 ng Ce
2.7 mmol α-HIBA
2SD
A
increased α-HIBA/Ce ratio
0.05
0.00
-0.05
-0.10
-0.15
-0.20
-0.25
δ146Nd (‰)
After chromatography
250 ng Nd
0.54 mmol α-HIBA
addition of α-HIBA
2SD
B

Fig. 11

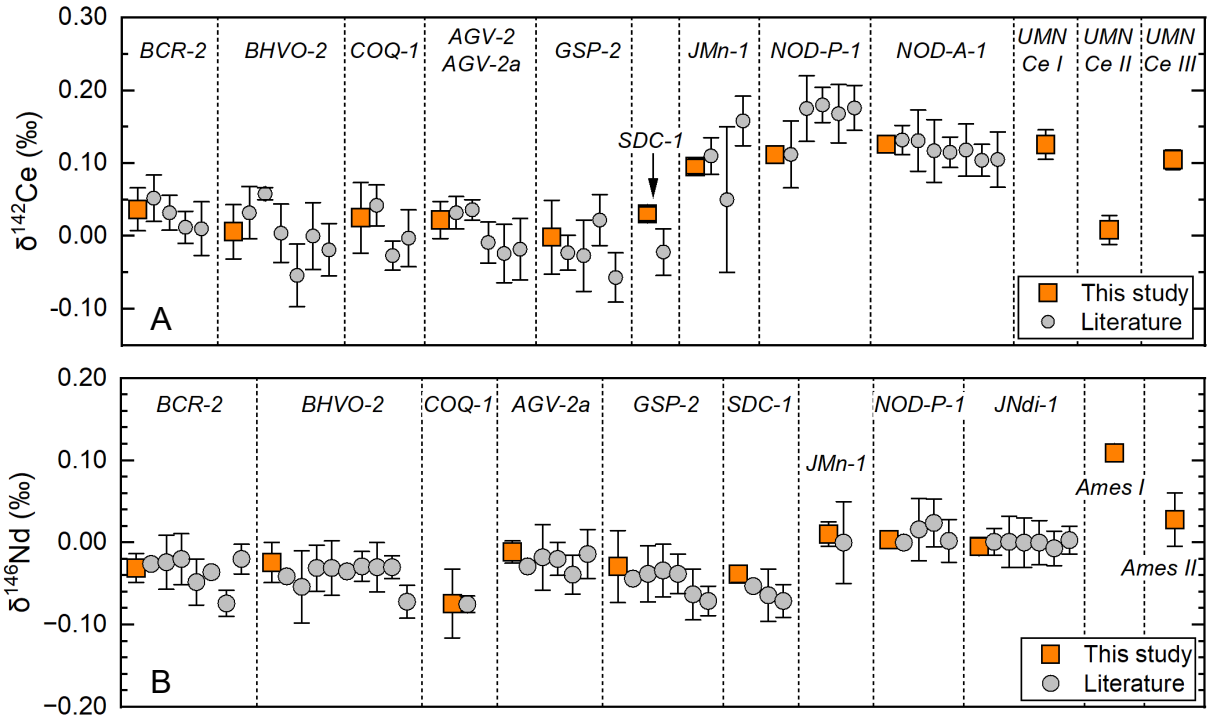
0.30
0.20
0.10
0.00
-0.10
δ142Ce (‰)
BCR-2
BHVO-2
COQ-1
AGV-2
AGV-2a
GSP-2
SDC-1
JMn-1
NOD-P-1
NOD-A-1
UMN Ce I
UMN Ce II
UMN Ce III
This study
Literature
A
0.20
0.10
0.00
−0.10
−0.20
δ146Nd (‰)
BCR-2
BHVO-2
COQ-1
AGV-2a
GSP-2
SDC-1
JMn-1
NOD-P-1
JNdi-1
Ames I
Ames II
This study
Literature
B

Fig. 12

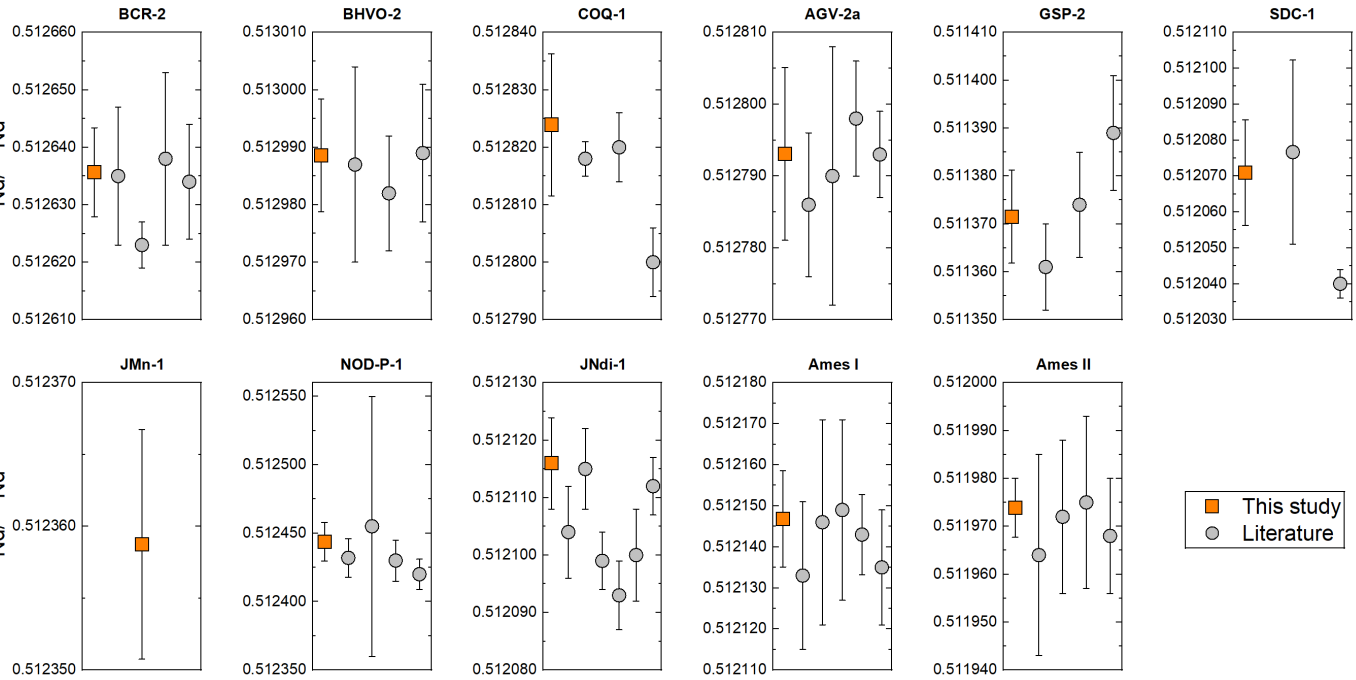
BCR-2
BHVO-2
COQ-1
AGV-2a
GSP-2
SDC-1
JMn-1
NOD-P-1
JNdi-1
Ames I
Ames II
$^{143}Nd/^{144}Nd$
This study
Literature

Table 1 Comparison of sequential Ce and Nd separation methods and their stable isotope analytical methods

					Ce				Nd			
Chromatographic method	**Automated system**	**Instrument**	**Plasma condition**	**Double spike[a]**	**Yield**	**Nd/Ce in Ce cut[b]**	**Blank (pg)**	**2SD[c] (‰)**	**Yield**	**Blank (pg)**	**2SD[c] (‰)**	**References**
AG50W-X8 + TRU + LN resins		Nu plasma 500 MC-ICP-MS	Dry plasma (Aridus)	N	98%	0.01-0.1%	<1,000	0.02-0.10	99%	<1,000	0.02-0.06	Ohno and Hirata (2013)
AG50W-X12 + DGA resins		Neptune Plus MC-ICP-MS	Wet plasma	N	99.3%	0.005-0.028%	48	0.034-0.046	99.5%	33	0.018-0.032	Bai et al. (2022)
DGA + LN resins	FPLC system	Neptune Plus MC-ICP-MS	Dry plasma (Apex Q+ Spiro TMD, Apex Omega, Aridus I)	N	>95%	-	<250	<0.1	>95%	<250	<0.1	Hu et al. (2021)
				Y	40-70%	-	-	0.08-0.036	40-70%	-	0.022-0.044	Hu et al. (2023)
AG50W-X8 + AG50W-X4 (α-HIBA) + DGA resins		Nu "Sapphire" MC-ICP-MS	Dry plasma (Apex Omega HF)	N	>99%	0.006-0.03%	46	0.009-0.051	>99%	2	0.01-0.042	This study

[a] N – no, Y – yes.
[b] Nd/Ce in Ce cut indicates total Nd/Ce mass ratios in the pure Ce cuts after chromatographic chemistry.
[c] Two standard deviations in $\delta^{142}Ce$ or $\delta^{146}Nd$ reported for a range of reference materials.

Table 2 The three-stage chromatographic procedure for sequential Nd and Ce separation

Eluent	Volume (mL)	Step
Column 1: pre-concentrate REE (Bio-Rad AG50W-X8 resin, 200-400 mesh, H^+ form)		
6 M HCl	10	Resin cleaning
Milli-Q water	5	Resin cleaning
2 M HCl	5	Resin conditioning
2 M HCl	1	Sample loading
2 M HCl	30	Washing
6 M HCl	28	REE collection
Column 2: Ce & Nd purification (Bio-Rad AG50W-X4 resin, 200-400 mesh, NH_4^+ form)		
Milli-Q water	0.2	Resin conditioning
0.1 M HCl	0.4	Sample loading
Milli-Q water	0.2	Washing
0.15 M α-HIBA pH 4.68	2.8	Washing
0.225 M α-HIBA pH 4.68	4	Washing
0.225 M α-HIBA pH 4.68	2.4	Nd collection
0.225 M α-HIBA pH 4.68	2	Washing
0.225 M α-HIBA pH 4.68	6.8	Ce collection
Column 3: α-HIBA removal from Ce & Nd cuts (Eichrom DGA normal resin, 50-100 µm, H^+ form)		
0.1 M HCl	2	Resin cleaning
Milli-Q water	1	Resin cleaning
4 M HNO_3	1	Resin conditioning
4 M HNO_3	1	Sample loading
4 M HNO_3	10 for Ce 4 for Nd	Washing
0.1 M HCl	6	Ce & Nd collection

Table 3 Faraday cup configurations for stable Ce isotope, stable and radiogenic Nd isotope measurements

	Faraday cups														
	H9	H8	H7	H6	H5	H4	H3	H2	H1	Ax	L1	L2	L3	L4	L5
Stable Ce isotope	^{148}Sm	^{145}Nd	^{144}Sm	^{142}Ce	^{140}Ce	^{139}La	^{138}Ce	^{137}Ba	^{136}Ce	^{135}Ba				^{131}Xe	
Potential interferences	^{148}Nd		^{144}Nd	^{142}Nd			^{138}La ^{138}Ba		^{136}Ba ^{136}Xe						
Stable & Radiogenic Nd isotope				^{153}Eu	^{151}Eu	^{150}Nd	^{149}Sm	^{148}Nd	^{147}Sm	^{146}Nd	^{145}Nd	^{144}Nd	^{143}Nd	^{142}Nd	^{141}Pr
Potential interferences						^{150}Sm		^{148}Sm				^{144}Sm		^{142}Ce	

Table 4 Instrument and data acquisition settings for stable Ce isotope, stable and radiogenic Nd isotope analyses

Settings	Stable Ce isotope, stable & radiogenic Nd isotope
Apex	
Ar sweep gas flow (L/min)	1.2~1.8
N_2 (mL/min)	4~6
Spray chamber temperature (℃)	140
Peltier cooler temperature (℃)	3
Desolvator temperature (℃)	155
Nebulizer gas (L/min)	0.7~0.9
Nebulizer uptake rate (μL/min)	100
Sapphire MC-ICP-MS	
Sampler cone	Nickel (0.9 mm hole), Part No. 319-646
Skimmer cone	Nickel (HS1-7), Part No. 325-294
Coolant (L/min)	13
Aux (L/min)	0.8~1.0
RF power (W)	1300
Acceleration (V)	~6000
Extraction (V)	~4000
Data acquisition	
Integration time (s)	5
Number of cycles per block	60
Washout time (s)	120
Uptake time (s)	65